ADVANCED INTELLIGENT SYSTEMS
Open Access
www.advintellsyst.com

Continuum Robots: An Overview

*Matteo Russo, Seyed Mohammad Hadi Sadati, Xin Dong, Abdelkhalick Mohammad, Ian D. Walker, Christos Bergeles, Kai Xu, and Dragos A. Axinte**

Herein, recent advances, current limitations, and open challenges in the design, modeling, and control of continuum robots are discussed. Thanks to their lean bodies, these robots achieve a long reach through narrow and tortuous environments, enabling currently unachievable tasks for medical, industrial, and service applications. The recent surge in research on these robots leads to significant advances in design, modeling, and control methods. Herein, these developments with a comprehensive review of existing continuum robots and emerging technologies are examined. Then, modeling and control approaches are compared, and navigation strategies exclusive to continuum robots, such as follow the leader, coiling, and circumnutation are examined. Finally, an overview of their applications is provided with a focus on industrial and service tasks, outlining open research challenges and future developments.

1. Introduction

When thinking of robots, the image that immediately springs to mind is either an android, designed to resemble human beings and mimic their behavior, or an industrial manipulator, for example, a large machine of rigid steel working in an assembly line. However, robotic systems of multiple forms have been developed to carry out the most diverse tasks, with designs that evolved from readily available structures, such as vehicles, or inspired by nature. In the last decade, more and more bioinspired designs have been enabled by advances in computer science, materials, and manufacturing. Among them, continuum robots, inspired by snakes, trunks, and tendrils, are characterized by a compliant backbone capable of continuous bending, whose shape (configuration, i.e., position and orientation along the backbone curve) is controlled by applying loads through onboard "intrinsic" actuators (e.g., pneumatics or hydraulics) or transmission elements (e.g., tendons, rods, or compliant tubes) that are pushed/pulled from an extremity of the backbone ("extrinsic actuation"). These robots have flexible bodies with a high length to cross-section diameter ratio and are uniquely suited to tasks that require the deployment of tools or sensors with a long reach into tortuous and narrow paths.[1]

Continuum robots were first developed in the 1960s[2] and rose to prominence in the late 1990s,[3] when they were often called elephant trunk,[4] tentacle/tendril,[5] or flexible[6] manipulators. Whereas other robots were characterized by intrinsic actuation and larger sizes, research on continuum robots first focused on miniaturization for medical applications,[7,8] leading to extrinsic actuation to enable leaner designs. Recently, continuum robots have been developed for a wider range of applications, including manufacturing, aerospace, search and rescue, and nuclear. In such scenarios, the infinite degrees of freedom (DoFs) of these slender robots enable inspection and intervention in areas that cannot be accessed by conventional robots (e.g., tunnels[9] and gas turbines[10]).

An exhaustive literature search (see Appendix) outlines a surging interest in continuum robots, with a 19.6% average annual growth in publications between 2012 and 2021 (continuum robot search on Web of Science). Three main topics can be observed in recent literature surveys,[11–36] listed in **Table 1**.

1.1. Design

Tendon-driven and concentric tube robots are predominant in surveys, but they are not the only design solutions.[18] This richer literature can be attributed to intense research effort toward medical and other small-scale applications when compared to larger-scale tasks (e.g., manipulation) where intrinsic actuation is advantageous.

M. Russo, X. Dong, A. Mohammad, D. A. Axinte
Faculty of Engineering
University of Nottingham
Nottingham NG8 1BB, UK
E-mail: dragos.axinte@nottingham.ac.uk

S. M. H. Sadati, C. Bergeles
School of Biomedical Engineering & Imaging Sciences
King's College London
London WC2R 2LS, UK

I. D. Walker
Department of Electrical & Computer Engineering
Clemson University
Clemson, SC 29634-0915, USA

K. Xu
School of Mechanical Engineering
Shanghai Jiao Tong University
Shanghai 200240, China

The ORCID identification number(s) for the author(s) of this article can be found under https://doi.org/10.1002/aisy.202200367.

DOI: 10.1002/aisy.202200367

Table 1. Surveys on continuum robots.

Topic	Covered in References	Years
General:		
-Soft and continuum robots	[1,3,11–14]	1999–2016
Design:		
-Tendon-driven robots	[15–18]	2017–2021
-Concentric tube robots	[15,19–22]	2016–2021
-Intrinsic actuation	–	–
-Stiffening solutions	[23,24]	2016–2018
Modeling and control:		
-Kinematics	[16,25,26]	2010–2021
-Statics and dynamics	[17]	2021
-Control	[27–31]	2018–2022
-Sensing	[32,33]	2017–2018
-Motion strategies	–	
Applications:		
-Medical	[21,22,32,34–36]	2015–2022
-Industrial and service	–	

1.2. Modeling and Control

From efficient geometrical models that assume piecewise constant curvature (PCC)[25] to more complex but accurate differential and finite-element methods (FEMs),[28] surveys on modeling outline different techniques and their application to model-based control. Other related topics, including model-less control[27] and sensing capabilities,[32,33] have been widely discussed. However, the discussion is limited to low-level control. High-level motion strategies (e.g., coiling or uncoiling, navigation, and circumnutation) are critical to many applications but have seen limited discussion.

1.3. Applications

The works in Table 1 either discuss theoretical aspects of continuum robots or narrow their analysis to medical robots.[34,35] While widely discussed in research papers, industrial and service applications are underrepresented in related surveys, and the wide variety of task requirements leads to a more fragmented research effort in those fields.

Therefore, three main gaps can be identified in previous continuum robot surveys: 1) a general overview on design, including intrinsic actuation, 2) a discussion of high-level motion strategies, and 3) industrial and service (i.e., nonmedical) applications. Furthermore, most recent works focus on specific aspects or medical applications rather than aiming at a perspective of the field as a whole. For these reasons, we present a broad overview on continuum robots, covering a wide range of design solutions, theoretical frameworks, and control strategies for medical, industrial, and service applications. By addressing the outlined research gaps and discussing new research trends, this work complements other recent reviews with a comprehensive outlook on the topic.

In Section 2, we provide a review of the existing design solutions for backbone and actuation. In Section 3, we discuss recent modeling and control trends, comparing common approaches. Sensing, control, and motion planning are discussed in Section 4. In Section 5, we analyze medical, industrial, and service applications. In Section 6, we outline open research challenges and discuss future developments and applications for continuum robots. The Appendix Appendix includes our methodology and a glossary with abbreviations/definitions.

2. Design

A continuum robot is typically defined as a continuously bending actuatable structure[1,34] with an extremity fixed to a base that can contain actuation and control hardware. The core element of a continuum robot is its backbone, which enables bending and acts as main structural component. Whether made of many compliant elements or a single flexible body, the backbone defines the overall shape of the robot.

Recent surveys classify continuum robots according to the nature of their backbone: in single-backbone robots, a central backbone runs through the whole length of the robot; multi-backbone robots are composed of a succession of rigid bodies (*vertebrae*) and flexible elements.[34] However, designs with multiple continuous backbones, such as rod-driven[37] or parallel[38] structures, elude this classification. We thus propose referring to robots with a continuously flexible body as continuous backbone robots, and to robots with an alternance of flexible and rigid elements as segmented backbone robots.

Backbone designs vary widely, from a continuous compliant element to a succession of rigid (or stiff) and compliant segments. The comprehensive design survey in ref. [18] identifies eleven joint architectures as a combination of compliant elements, including tubes, beams, springs, blades, bellows, origami structures, and braids. However, classifying backbone designs is a challenging task, as different architectures often overlap and are intertwined with the underlying actuation principle.

A further distinction can be made from how the robot is actuated: intrinsic actuation is embedded along the backbone, whereas extrinsic actuation is located at one extremity (generally fixed at the base of the robot). In this section, we characterize continuum robots according to these actuation categories, presenting advantages and disadvantages, describing typical backbone architectures for each type of actuation, and outlining emerging design solutions.

2.1. Extrinsic Actuation

In continuum robots with extrinsic actuation, motion is generated from the base of the backbone and transmitted along it by mechanical elements. This solution is particularly convenient for small scale applications: as the size of the robot's body is not constrained by the size of the motors, the cross-section diameter can be extremely small (3 mm or less). However, this also increases modeling complexity, as actuation variables require an additional model "layer" to be mapped onto the shape of the backbone.

Three broad families of continuum robots with extrinsic actuation are characterized by specific transmission elements:

1) Tendon-driven continuum robots are actuated with sets of tendons routed along the backbone (**Figure 1**a–d). 2) Concentric tube continuum robots are made of pre-curved tubes nested inside of each other, whose shape is controlled by translating and rotating each tube (**Figure 2**a,b). 3) Rod-driven continuum robots are actuated by pulling and pushing rods that act as parallel backbones (Figure 2c,d).

2.1.1. Tendon-Driven Continuum Robots

In a tendon-driven continuum robot, the backbone is bent by pulling tendons from its fixed extremity. The main elements of tendon-driven continuum robots are as follows:

Vertebrae: Vertebrae, or disks, are rigid elements along the backbone. With their geometry, these bodies route tendons, electrical wires, and tools along the backbone. Their outer diameter often defines the diameter of the robot, and they often include a channel to deliver tools to the robot's tip.

Flexible Elements: The vertebrae of the robot are connected through flexible elements, which are usually rods or lamellae made of superelastic materials, such as nickel–titanium alloys (NiTi or nitinol).

Tendons: The motion of the robot is controlled by pulling tendons. Groups of tendons are fixed at specific vertebrae and bend the backbone up to that point. By terminating tendon groups at different lengths of the body, the backbone is divided into segments (also known as sections) that can be independently actuated. Planar and 3D motions require two and three tendons per segment, respectively. Conventionally, when the backbone is straight, the vertebrae align along a straight cylindrical channel to simplify tendon installation, but irregular layouts have also been proposed.[39,40]

Many early (e.g., refs. [1,41]) and recent (e.g., ref. [42]) tendon-driven continuum robots have a single continuous backbone, as shown in Figure 1a,b.[34] The vertebrae of these single-backbone robots are mostly used for tendon routing, whereas the vertebrae of robots with segmented backbones are also structural elements. Alternative backbone solutions to an elastic rod include tubes with V-shaped notches[43] or tendon-driven braids.[44] These designs have large internal channels but nonuniform stiffness.

Continuum robots with a segmented backbone (Figure 1c,d) can only approximate a continuous curvature. Vertebrae are integral to their segmented backbones made of many flexible elements between rigid bodies, such as hinges made of two lateral elastic elements (e.g., twin-pivot designs[45,46] and compliant hinges[47]) or coil springs,[48,49] which can also be used to control segment extension. This design results in approximations when studied with continuous models but allows for empty space at the center of each vertebra, creating a channel for delivering tools at the robot's tip.

2.1.2. Concentric Tube Robots

Concentric tube continuum robots (Figure 2a,b), also known as *active cannulas*, are made of pre-curved tubes with decreasing

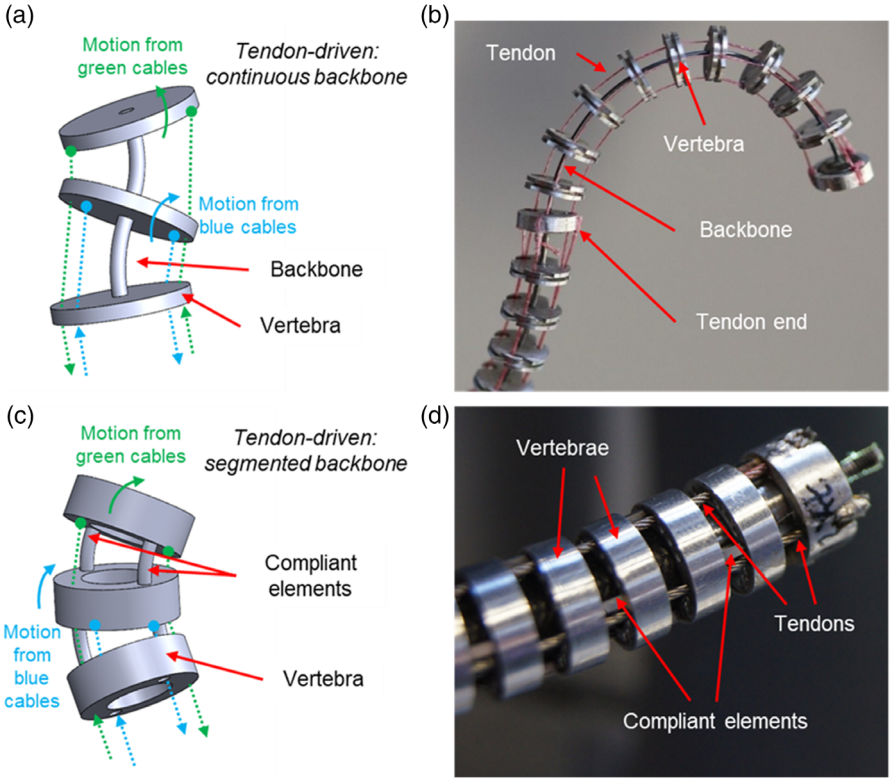

Figure 1. Continuum robots with extrinsic actuation: a) a tendon-driven design with continuous backbone and b) an example prototype; Reproduced with permission.[42] Copyright 2021, SAGE Publications; c) a tendon-driven robot example of segmented backbone robot structure, d) with multiple elastic elements in a twin-pivot configuration as per prototype.[45,46]

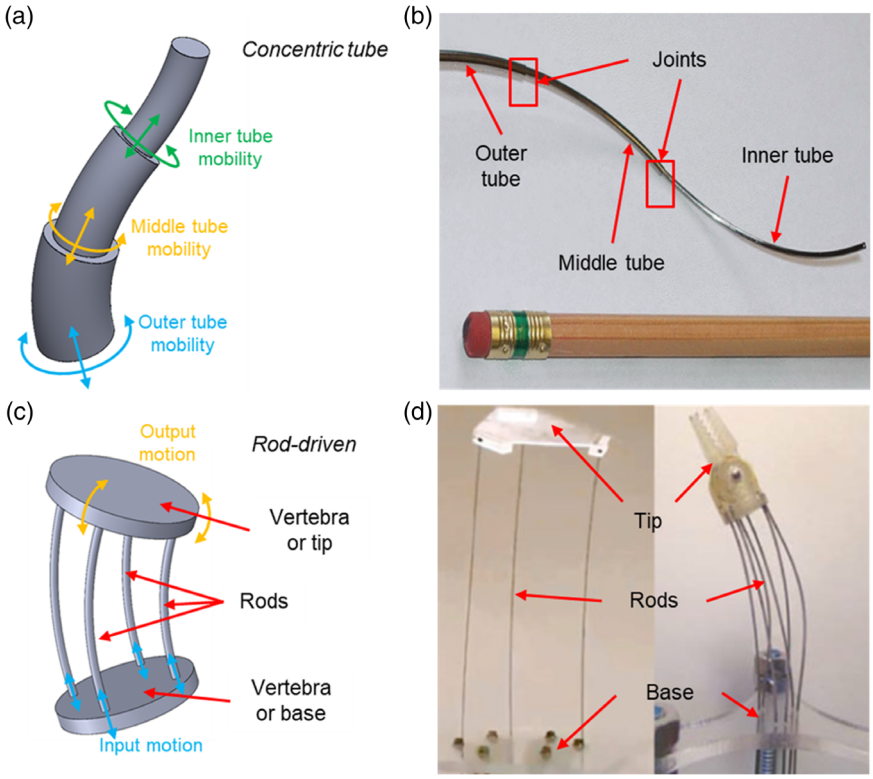

Figure 2. Continuum robots with extrinsic actuation: concentric tube robots, a) with their mobility and b) a prototype; Reproduced with permission.[50] Copyright 2010, IEEE; rod-driven continuum robots, c) with a conceptual scheme and d) a parallel continuum robot prototype. Reproduced with permission.[38] Copyright 2018, IEEE.

diameter and increasing length nested within each other and grasped at their respective bases by actuators that provide axial rotation and translation for insertion and retraction.[19–22,50] By interacting elastically with each other, these tubes elongate and bend. Two elements characterize concentric tube robots:

Tube: Nested tubes, often from NiTi, are the structural element of a concentric tube robot and act as its backbone.

Coaxial Actuation Unit: Concentric tube robots are externally actuated and require two dedicated motors (rotation and translation) per nested tube to control the system. Given the particular design, all these motors need to be coaxial.

The main appeal of concentric tube robots is the smallest outer diameters out of all the continuum robots, making them suited to surgical applications.[20] However, as two independent motors are needed for each actuator, this design is difficult to upscale (as the serial architecture of these robots implies a larger absolute tip error for a longer backbone), and control is affected by structural elastic instabilities. Alternative designs with helical pre-curvature[51] or patterned tubes[52,53] improve performance, and hybrid designs with features from both concentric tube and tendon-driven robots have been recently developed.[54,55]

2.1.3. Rod-Driven Continuum Robots

Rod-driven continuum robots (Figure 2c) are similar in design to their tendon-driven counterparts. By replacing tendons with rods, the backbone shape can be actuated not only by pulling but also by pushing (as rods work both in tension and compression). Their control strategy resembles concentric tube robots instead, as a desired end-effector pose is achieved with an equilibrium modulation by changing the inserted length of the rods.[37,56] By actuating the backbones directly, rod-driven robots can achieve not only bending through antagonistic actuation but also elongation through concurrent actuation.[37] Furthermore, rods can be used to actuate parallel continuum robots (Figure 2d), as detailed in Section 2.3.[38]

2.2. Intrinsic Actuation

Continuum robots with intrinsic actuation are characterized by a direct local control over the backbone shape. Common intrinsic actuation technologies rely on a pressurized working fluid, but shape-memory alloys (SMA), dielectric actuators, and other smart materials can also be used.[14] Onboard actuation usually increases robot size, making it unsuitable for small-scale applications. However, when compared to designs with extrinsic actuation, a better force transmission efficiency (and thus potentially higher payloads) can be achieved, and modeling and control are simplified. Research on smart material actuators has been scattered, but pneumatics has been successful with two main designs: 1) Fluid muscle robots, intrinsically actuated with a pressurized fluid in antagonistic soft chambers (**Figure 3**a,b). 2) Soft

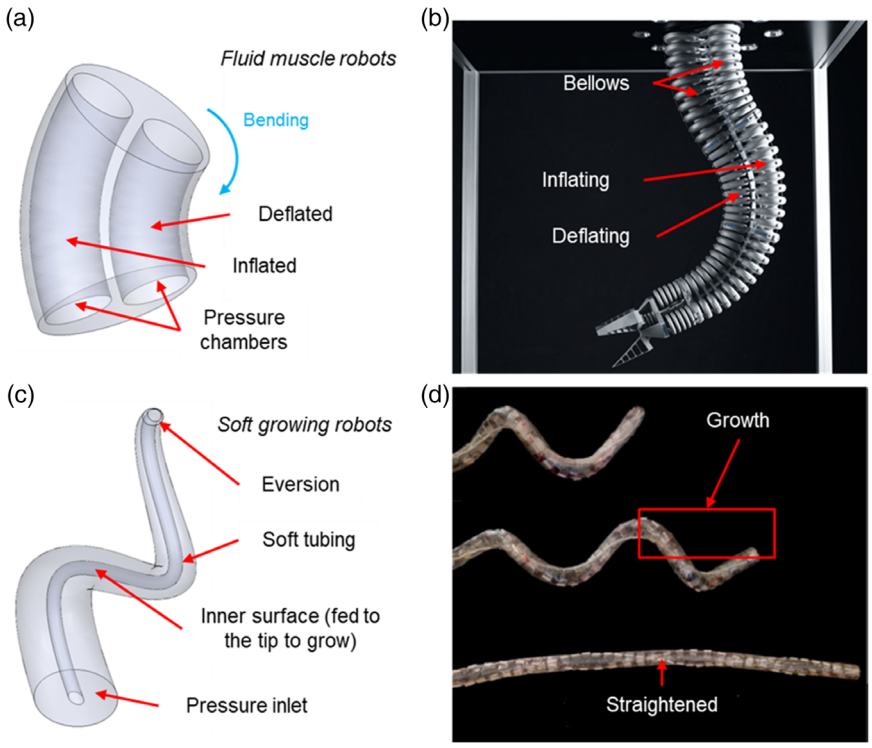

Figure 3. Continuum robots with intrinsic actuation: a) conceptual diagram of fluid muscle actuation and b) a bellows-based example; Reproduced with permission.[61] Copyright 2017, IEEE; c) soft growing robot concept and d) an example prototype. Reproduced with permission.[62] Copyright 2018, IEEE.

growing robots, able to increase their length, usually intrinsically actuated with pneumatics (Figure 3c,d).

Differently from other intrinsic actuation technologies, magnetic fields can also be directly used to control backbone shape without an increase in robot size.[36,57,58] However, this solution suffers from environmental interference and only a low force can be transmitted, making it suited to a limited range of applications (mostly medical[58]).

2.2.1. Fluid Muscle Robots

Fluid muscle robots replicate the behavior of antagonistic muscles with pressurized chambers (e.g., bellows) that bend the backbone by alternatively inflating and deflating (Figure 3a,b).[59,60] These robots, developed for almost three decades, are characterized by both continuous[61] and segmented[59] backbone designs. A high payload makes them suited to manipulation tasks in unstructured environments.

2.2.2. Soft Growing Robots

Soft growing robots are an innovative design with intrinsic actuation. By combining the flexibility of continuum robots with the capability to significantly extend the length of their backbone, growing robots can achieve a reach of tens of meters with a small compliant form factor thanks to their eversion capability.[9] Specifically, growth is achieved by using a soft tubing folded into itself (Figure 3c,d), resulting in a pressurized inlet between its internal and external surfaces. The external surface is fixed at the base, while the internal surface is free to translate. As such, when pressure in the inlet is increased, a portion of the internal surface unfolds at the tip with an eversion motion, becoming the external surface and thus increasing the overall length of the robot.[62–66] While growth enables long-reach applications such as search and rescue, this design is hindered by low accuracy, payload, and motion controllability.

2.3. Complementary Design Considerations

2.3.1. Stiffening Solutions

The structural behavior of a continuum robot resembles a cantilever beam, with an unconstrained length fixed at one end and a small cross section. Thus, any wrench applied to the system, including the robot's weight, can impose a significant deflection. Even if modeling can compensate for this deflection[67] and related consequences (e.g., backbone torsion[68]), these issues are better mitigated by stiffening the robot.[23,24] However, high compliance is desirable in continuum robots, and an intrinsically high stiffness would be detrimental. As such, several technologies have been developed to modulate backbone stiffness, based on the following working principles:

Material Jamming: Jamming-based systems (**Figure 4**a) require a membrane filled with a granular media or thin sheets. By applying a vacuum, the membrane collapses on the filler, increasing its density and stiffness. Jamming-based technologies are simple, are reliable, and achieve local stiffening after reaching the desired

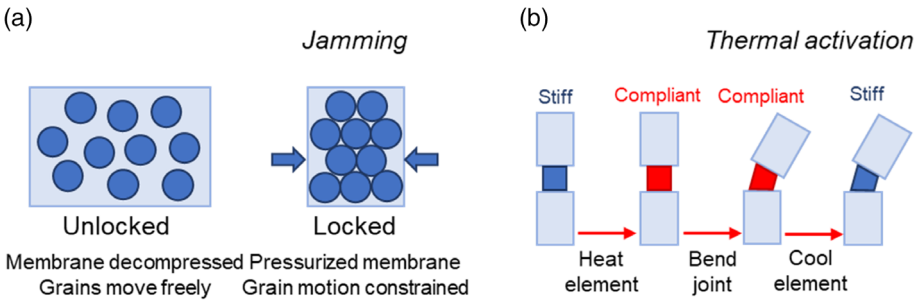

Figure 4. Solutions for continuum robot stiffening: a) material jamming principle; b) an example of low-melting element activation and stiffening.

position.[69,70] However, the stiffening element can be difficult to include without significantly increasing the size of the robot.

Thermal Activation: Materials with a low melting point can be heated to a phase change to modulate stiffness in the compliant elements (Figure 4b) or with an external sleeve.[71,72] SMA or polymers can be similarly used.[73,74] As the thermal activation is triggered by Joule heating, size scaling is not an issue. However, the required activation and cooling time hinders real-time applications, and the consequent thermal field could affect robot performance.

Mechanical Design: A continuum robot can tune its stiffness by varying its diameter with a reconfigurable mechanism;[75] locking tendons along the backbone;[76] integrating a movable stiffer element into the backbone;[77,78] or exploiting an anisotropic distribution of the flexural stiffness of the structure.[79]

2.3.2. Parallel Continuum Robots

Our definition of continuum robots implies a serial architecture with a single kinematic chain going from a fixed base to the tip. However, multiple independent continuum kinematic chains in a parallel configuration can control the position of a rigid body (Figure 2d), resulting in a smaller workspace but higher stiffness, repeatability, and speed. This idea is relatively recent,[80] but planar[81] and 3D[82] parallel continuum robots have reported promising performance.[83] The main challenge of these robots is coordinating the motion of multiple limbs to obtain a controlled motion.[84–86] However, their compact (rather than slender) shape factor prevents their use in remote tasks through narrow passages.

2.3.3. Untethered Continuum Robots

Continuum robots with untethered actuation (i.e., generating motion without a physically tethered connection) would elude the proposed definitions by removing the need for a fixed platform at the robot extremity, potentially enabling snake-like locomotion[87] and providing further scalability to continuum technologies. While not untethered yet, magnetically actuated continuum robots[88,89] represent a first step in this direction, and further developments are likely in the near future.

2.3.4. Evaluating Designs

The performance of continuum robot designs is usually assessed with specifications and indicators developed for rigid-link robots.[90] These indicators include precision (or error)[16,91] and Jacobian-based metrics,[92,93] generally focusing on end-effector behavior. As such, they can hardly capture the performance of the entire robot, only characterizing the segment of the robot that provides up to six DoFs at the tip and neglecting the behavior of the rest of the backbone.

From a geometrical perspective, the key specifications of a continuum robot are backbone length, cross-sectional diameter, and minimum bending radius. These design parameters define how a continuum robot can move in a complex environment: the width of the narrowest passage along the desired path must be larger than cross-sectional diameter; the sharpest bend along the path must have a radius of curvature larger than the minimum bending radius of the backbone; and the length of the desired path must be shorter than the length of the backbone. The ratio between backbone length and cross-sectional diameter has been often used as an index to evaluate the form factor of a continuum robot, sometimes called slenderness (e.g., in ref. [35]).

Physically, these geometrical parameters are constrained by design features. A smaller cross-sectional diameter is generally seen as favorable, but as the cross section must fit the actuation elements, sensors, tools, and sometimes an empty inner channel to fit the end-effector; the encumbrance of all these components (and their relative design and manufacturing tolerances) determines the minimum value for the cross-sectional diameter. A longer backbone length implies larger friction and energy losses when transmitting power throughout the backbone, as well as a lower stiffness and thus payload. The minimum bending radius of the backbone is constrained by internal collisions, actuation limits, and material mechanics.

As discussed in Section 2.3.1, another critical specification of a continuum robot is its stiffness, which determines the payload at the end-effector as well as if the robot is able to operate in a fully suspended configuration or requires local contacts as supports, thus totally changing its functionality. As such, the stiffness of the robot, conceived as the ratio between an applied load and the corresponding deflection of a segment of backbone, can be used as a performance index. Given the complexity of a continuum robot design, which often includes some elements that contribute to the overall stiffness but are almost impossible to model (e.g., power cables that are routed from the base of the robot to the end-effector through an inner channel), an experimental evaluation of the stiffness coefficient is often preferred, as for example reported in refs. [94,95].

3. Modeling

The behavior of a continuum robot is mathematically represented by modeling its configuration (kinematics), defined as the set of positions that fully describes system geometry, according to system (governing equations or conservation laws derivation method) and material mechanics (constitutive laws). Recent surveys have proposed compelling categorizations, mostly based on system kinematics, to classify relevant modeling techniques.[26,29] In this survey, we adapt a systematic approach based on the standard convention in classic continuum mechanics research, thus classifying methods according to the following: 1) Kinematics, which define the robot configuration with either absolute[96–98] or relative[99] coordinate frames. Absolute models refer to a fixed inertial frame, whereas relative models define the configuration in relative frames that depend on the robot's motion. As such, absolute frames simplify the description of interacting with the environment, whereas relative frames are conveniently employed for actuation and proprioception. 2) System mechanics, which define how the potential fields in the system (e.g., gravitational and elastic deformation energy) reach an equilibrium to steer the system's kinematics. Common formulations for system mechanics include the principle of virtual work (PVW) and the Lagrangian method. 3) Material mechanics, which define the system deformation energy through constitutive laws (e.g., Hooke's law) that relate material strain (bending, torsion, shear, and elongation) to wrench or stored energies.

Various combinations of techniques for kinematics, system mechanics, and material mechanics can be used to model a continuum robot. Some combinations are widespread (e.g., continuously variable curvature (VC) kinematics with Cosserat rod theory and Hooke's law). Hybrid solutions have also been proposed (e.g., Lagrangian dynamics based on Cosserat rod formulation[99]). **Table 2** provides a list of analytical modeling techniques (i.e., excluding data-driven approaches).

Table 2. Elements of continuum robots modeling.

Kinematics:	
Continuous kinematics:	Discrete kinematics:
-Variable curvature (Cosserat)[100–104]	-Relative states:
-Modal (fitting, reduced order):	*Pseudo rigid Body chain*[16,119]
*Shape fitting[111–115]	*Piecewise constant strain (PCS) or curvature (PCC)[98,119,120]
*Strain fitting, piecewise variable strain (PVS)[105–110]	-Absolute states:
	*Absolute nodal coordinate formulation (ANCF)[96–98]
Mechanics:	
System (conservational law) derivation:	Material (constitutive law):
-Cosserat rod[100–103,116,117]	-Hooke's law[100,133]
-Euler–Bernoulli beam[131,132]	-Finite strain (hyperelasticity):
-Principle of virtual work[97,116]	*Neo-Hookean[116,117,119]
-TMT[98,111,112]	*Mooney–Rivlin[136]
-Lagrangian dynamics:	*Gent[119]
*Continuous[104,106,133]	-Hyper viscoelasticity:
*Lumped mass[118,134,135]	*Kelvin–Voigt[104]
-Recursive computation[99,133]	*Viscosity power law[98,111]

In this section, we provide an overview on these techniques with example of popular (PCC, Cosserat Rod) and emerging (modal, fitting) techniques. We also report complimentary considerations, such as friction modeling and cross-section deformation, and overview learning-based methods. A detailed discussion on specific aspects of modeling can also be found in recent surveys.[25–30,98]

3.1. Kinematics

The shape of the backbone can be modeled as a continuous differentiable curve or as a series of discrete elements (**Figure 5**). Continuous kinematic representations result in a set of partial differential equations (PDEs) with differential states for the system's equation of motion (EoM), and are divided in the following:

VC models: which provide an exact formulation based on a continuum mechanics model of system energy, with a continuous, infinite-dimensional configuration space. Example of such continuum mechanics models are Cosserat, Kirchhoff, and Euler–Bernoulli rod/beam theories.[100–104]

Modal techniques (reduced-order model—ROM): which provide a shape function based on the approximation of the robot backbone strain,[105–110] shape,[111–115] or cross-section geometry deformation[116,117] via a shape-fitting technique (e.g., cubic spline, Bezier) or a weighted sum of differentiable shape functions (known as system modes). As a result, a differentiable finite state-space system is formed to benefit from conventional rigid-body robot modeling and control techniques. Constant curvature methods[25,118] could be considered a special case of such shape approximation techniques.

Discrete (piecewise) kinematics approaches: which provide an approximation of the robot kinematics with discrete rods, pseudo rigid bodies (PRB), lumped masses, or other elements. While generally less accurate than continuous techniques, discrete models are appealing as they enable the application of rigid robotics kinematic models and control methods to continuum designs. In this regard, discrete techniques include the following:

PRB kinematics: with the backbone modeled as a highly articulated rigid chain; PRB kinematics approximates the robot backbone as a highly articulated rigid-body chain with elastic rotational and translational joints.[16,119]

Piecewise constant strain (PCS): with local strains as relative states. The widespread PCC method is a special case of PCS where all the states but bending (i.e., elongation, shear, and torsion) are set to zero. PCC represents the system as a series of constant curvature elements, where the system kinematics is derived by discretizing VC relations,[98] or employing equivalent elastic joints.[120]

Absolute nodal coordinate formulation (ANCF): with absolute nodal coordinates (both position and orientation) as the system states. The ANCF method employs a FEM-like framework in which Euler–Bernoulli beam[98] or cubic polynomial fitting[96] can be employed to derive the element strain from the absolute states. Rotation matrices,[119] quaternions,[98] or screw theory[120–122] are employed to represent frame transformations between the elements.

Both PCS and ANCF can employ a modal (shape function) representation, such as constant curvature or a cubic polynomial curve, to represent the individual element kinematics.

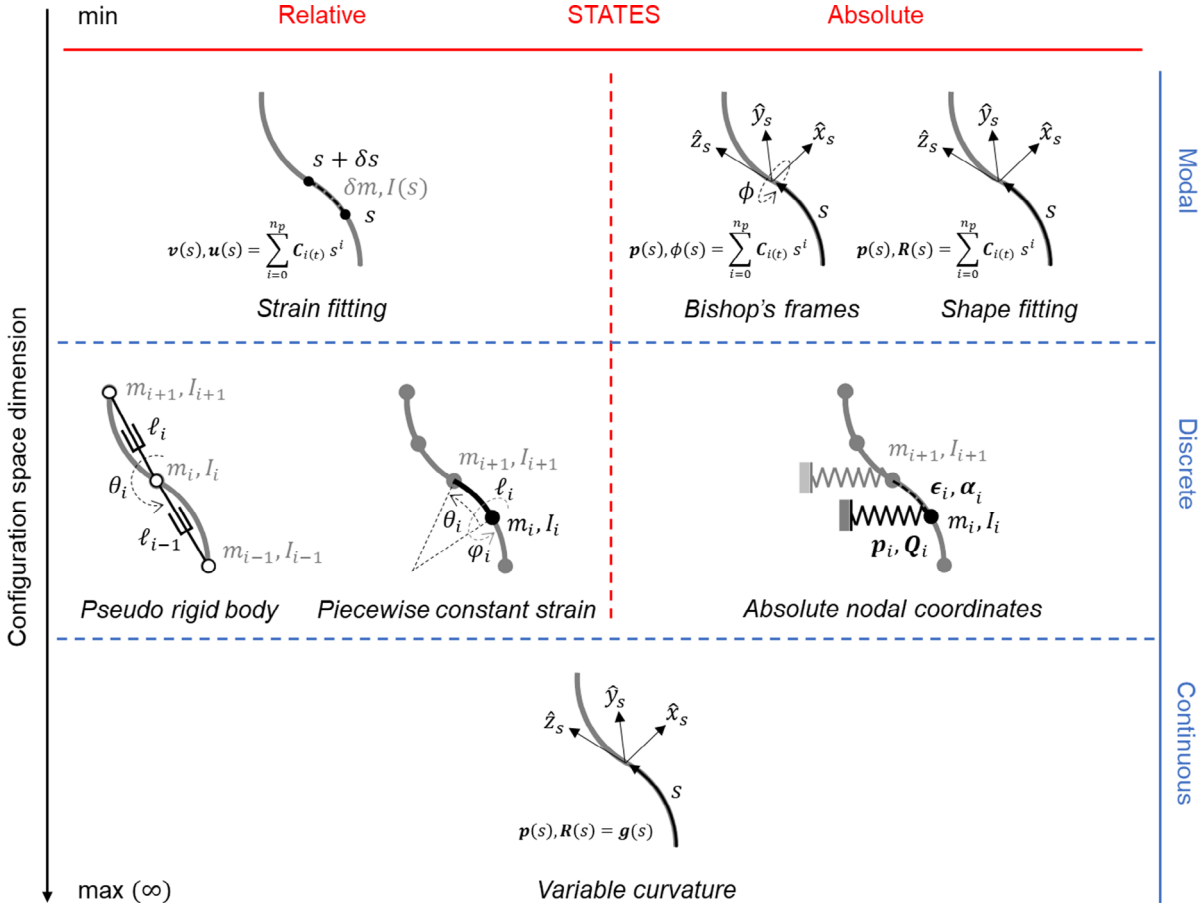

Figure 5. Continuum robot kinematics can be represented with modal (reduced order) parametrization, discretization, or a continuous formulation. General shape (position and orientation) fitting, Bishop's frame correction twist angle fitting, and strain fitting (with piecewise variable curvature) are instances of modal techniques. Piecewise constant strain/curvature kinematics (series of beams with relative state transformations) and absolute nodal coordinate formulations (finite-element-like series of lumped masses connected by Euler–Bernoulli beams or polynomial curves) are instances of discrete piecewise techniques with a modal-based (shape function) representation of individual element kinematics. Pseudo rigid body kinematics is a different instance of discrete techniques.

Here, we report four common models (PCC, ANCF, Cosserat rod theory, and reduced order) with their general formulations (nomenclature in **Table 3**) as examples of discrete and continuous kinematics.

3.1.1. Piecewise Constant Curvature

Even if multiple models for continuum robots have been proposed, constant curvature assumptions are widely used thanks to their simplicity and rich literature.[25] Naturally, constant curvature is rarely observed in reality[28,29,117] due to the presence of external and body loads, torsional strains, tendon friction, nonlinear material behavior, fabrication, and other issues. Nevertheless, a variable backbone curvature can be approximated by discretizing the backbone curve into multiple constant curvature segments with relative (PCC[25]) or absolute (FEM-like[96,97]) states.

Thus, the PCC approach models the shape of a continuum robot with a succession of circular arcs with curvature that is constant in space but variable in time. As per **Figure 6**a, each arc is defined by three independent variables, which describe the arc length ℓ, the underlying bending angle θ, and the direction of bending φ. The resulting curve describes the backbone of the robot and is characterized by a continuous differential (i.e., consecutive segments share the same tangent at their shared end). Furthermore, the cross section of the robot is usually assumed to be rigid and normal to the tangent of the backbone.

The base of the robot is defined by a fixed orthonormal basis field ("frame") $\{S_0\}$, while the terminal vertebra of the ith segment is defined by frame $\{S_i\}$. The transformation $T^i_{i-1} \in \mathrm{SE}(3)$ from $\{S_{i-1}\}$ to $\{S_i\}$ can be expressed by

$$T^i_{i-1} = \begin{bmatrix} R^i_{i-1} & \mathbf{t}^i_{i-1} \\ 0_{1\times 3} & 1_{1\times 1} \end{bmatrix} \tag{1}$$

where $R^i_{i-1} \in \mathrm{SO}(3)$ is the rotation and $\mathbf{t}^i_{i-1} \in \mathbb{R}^3$ is the translation along the arc that describes the segment. When parametrizing the motion by bending direction φ and angle θ, as in Figure 6a, the rotation from $\{S_{i-1}\}$ to $\{S_i\}$ can be written as

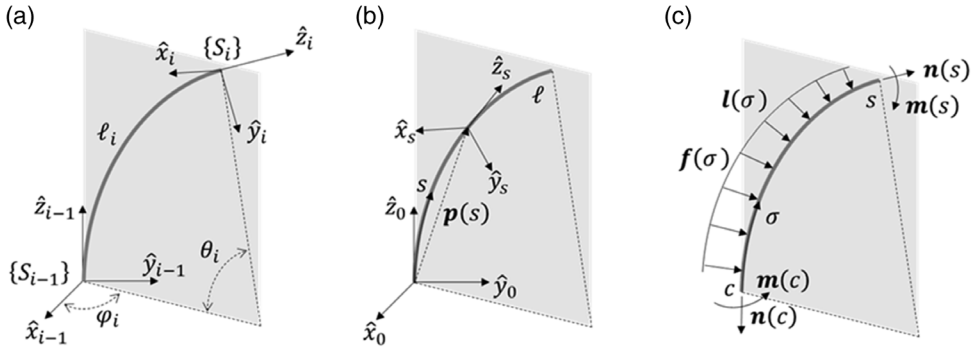

Figure 6. Continuum robot kinematics: a) piecewise constant curvature (PCC) scheme of the *i*th segment of a continuum robot; b) Cosserat rod kinematics; c) Cosserat free-body diagram of a backbone segment from arc length *c* to *s*, subject to internal and distributed forces and moments.

$$R_{i-1}^{i} = R_z(\varphi_i)\cdot R_y(\theta_i)\cdot R_z(-\varphi_i) \tag{2}$$

and the corresponding translation can be written as

$$\mathbf{t}_{i-1}^{i} = \frac{\ell_i}{\theta_i}\begin{bmatrix}\cos\varphi_i(1-\cos\theta_i)\\ \sin\varphi_i(1-\cos\theta_i)\\ \sin\theta_i\end{bmatrix} \tag{3}$$

where ℓ_i is the length of the backbone from $\{S_{i-1}\}$ to $\{S_i\}$.

This model is limited by a kinematic singularity whenever any segment of the robot is in a straight configuration ($\theta_i = 0$), since Equation (3) cannot be defined. However, this discontinuity is a mathematical artifact caused by the model and does not reflect an unstable physical behavior in that configuration. Different parametrizations can circumvent this issue. A Bishop's frame formulation, for example, defines two bending values around the axes of a segment's local frame ($\mathbf{u}_x = \partial\theta_x/\partial s$, $\mathbf{u}_y = \partial\theta_y/\partial s$), and a twist $\mathbf{u}_z = \partial\phi/\partial s$.[119] Alternatively, singularity-free modal approaches can be used.[107,114,115]

3.1.2. Absolute Nodal Coordinate Formulations

In PCC discretization, consecutive segments relate via compliant joints which are moving according to local strains. In FEM-like ANCF kinematics, nodes are defined with their Cartesian position and quaternion representation of orientation as the system absolute states.[96,98] To calculate the system deformation energy, an element's local linear strain (shear and elongation) ε_i and bending/twist angle vector $\boldsymbol{\alpha}_i = [\theta_x,\ \theta_y,\ \phi]$ are calculated based on the inverse map.

$$\varepsilon_i = Q_i^{-1} * (\mathbf{p}_{i+1} - \mathbf{p}_i) \tag{4}$$

$$[0,\ \boldsymbol{\alpha}_i] = 2Q_i^{-1} \times (Q_{i+1} - Q_i) \tag{5}$$

where $\times$ and $*$ denote respectively the quaternion multiplication and rotation of a vector as defined in refs. [98,123], Q_i is the element's absolute orientation quaternion, and $\mathbf{p}_i$ the element's position vector. This map is obtained by linearizing the inverse VC kinematics of a curve.[98] The difference between an ANCF and standard FEM kinematics is in the calculation of bending and twist, explicit in ANCF. This makes ANCF more suitable for modeling 1D elements such as continuum rods, as FEM relies on the deformation of a 3D position field (mesh) to detect changes in orientation.

Both PCC and ANCF kinematics result in a finite-dimension system that enables the use of rigid-body techniques for nonlinear controller design and dynamic system analysis. Conversely, geometrically exact modeling, which reproduces the exact deformation nonlinearity with no approximation to kinematic variables, usually relies on differential VC with an infinite number of states[100] as follows.

3.1.3. VC Kinematics (Cosserat Rod)

VC kinematics with Cosserat rod theory describes the configuration of a flexible rod as a framed curve[100] (Figure 6b). Like ANCF, VC kinematics considers both bending and twist actions along the backbone curve but using relative states instead. A Cosserat rod is defined by its centerline, which is the spatial curve of its mass centroid $\mathbf{p}:[0,\ell] \to \mathbb{R}^3$. This curve is arc-length parametrized in its initial configuration, yielding $\|\mathbf{p}'(s)\| = 1\,\forall s \in [0,\ell]$, where $\mathbf{p}'(s)$ is the tangent vector at parameter value *s*, defined as $\mathbf{p}'(s) = \partial\mathbf{p}/\partial s$ and the length of the curve is given by

$$\ell = \int_0^{\ell} \|\mathbf{p}'(s)\| ds \tag{6}$$

Cosserat rod theory assumes a rigid cross section of the rod that is not necessarily normal to the tangent of the centerline curve (differently from traditional Euler–Bernoulli beam theory, Kirchhoff rod theory, and PCC), thus modeling also shear deformation. To describe the evolution of the orientation of the cross sections along the rod, a frame can be defined as

$$R:[0,\ell] \to \mathrm{SO}(3) \tag{7}$$

Therefore, a continuum robot can be modeled as a parametrized homogeneous rigid-body transformation $g(s) \in \mathrm{SE}(3)$ with centerline position $p(s) \in \mathbb{R}^3$ and cross-section orientation $R(s) \in \mathrm{SO}(3)$ with respect to arc length *s* as

Table 3. Nomenclature.

Symbol	Description
Piecewise constant curvature	
n	Number of segments
i	Segment index
ℓ_i	Segment length
θ_i	Segment bending angle
φ_i	Segment direction angle
$\{S_0\}$	Base frame
$\{S_i\}$	Terminal vertebra frame
$\mathbf{t}^i_{i-1}$	Translation vector from $\{S_{i-1}\}$ to $\{S_i\}$
R^i_{i-1}	Rotation matrix from $\{S_{i-1}\}$ to $\{S_i\}$
T^i_{i-1}	Transformation matrix from $\{S_{i-1}\}$ to $\{S_i\}$
$\mathbf{p}_i$	Position vector of the origin of frame $\{S_i\}$
Absolute Nodal Coordinate Formulation	
i	Element index
ε_i	Element'[s] local linear strain
$\boldsymbol{\alpha}_i$	Element'[s] bending/twist angle vector
θ_x, θ_y	Bending angles
ϕ	Twist angle
Q_i	Element'[s] absolute orientation quaternion
$\mathbf{p}_i$	Element'[s] position vector
Variable Curvature—Cosserat Rod Theory	
s	Arc-length parameter of $\mathbf{p}$
ℓ	Curve length
$\mathbf{p}(s)$	Position of mass centroid
$R(s)$	Frame rotation
$g(s)$	Frame transformation
$\nu(s)$	Linear rates of change of $\mathbf{p}(s)$ in the local frame, i.e., strains
$\mathbf{u}(s)$	Angular rates of change of $R(s)$, i.e., curvature and torsion
$n(s)$	Internal force acting on cross section [s]
$m(s)$	Internal moment acting on cross section [s]
$f(s)$	Distributed external force acting on cross section [s]
$l(s)$	Distributed external moment acting on cross section [s]
ρ	Material density
a	Rod cross-section area
j	Rod [second] moment of area
ω	Local angular velocity expressed in global frame
t	Time
Modal Kinematics	
n_p	Fitting order
$\mathbf{C}_{i(t)}$	Time variant coefficient vector
s^i	Polynomial shape (basis) function

$$g(s) = \begin{bmatrix} R(s) & \mathbf{p}(s) \\ 0 & 1 \end{bmatrix} \tag{8}$$

The linear and angular rates of change of $g(s)$ with respect to s can be represented by variables $\nu(s)$ and $\mathbf{u}(s)$, respectively. The evolution of $g(s)$ along s can be then written as

$$R'(s) = \frac{\partial R}{\partial s} = \hat{u}(s)R(s), \quad \mathbf{p}'(s) = R(s)(\nu(s) + \mathbf{p}'_0) \tag{9}$$

where $\hat{\mathbf{u}}(s)$ represents the transformation of the $\mathbf{u}(s)$ vector in $\mathbb{R}^3$ into a skew-symmetric matrix $\mathrm{so}(3)$, and $\mathbf{p}'_0 = [0,\ 0,\ 1]$ is the tangent unit vector at the base to define the rod's initial direction (here along the global frame z-axis).

Overall, Cosserat rod theory provides a geometrically exact model for continuum robots, although a geometrically exact solution can also be sought with a finite difference formulation.[124] A Cosserat model has been proven to accurately predict the shape of a physical prototype within 2% of the robot total length[101] when considering both the actuation and the wrench acting on the robot. However, it is more complex than PCC, resulting in an infinite state-space system not fitting well-known rigid-body robotics concepts and requiring spatial integration steps that can be computationally expensive. Hence, this is a challenge to overcome for real-time control. To address this issue while preserving modeling accuracy, reduced-order interpolation and fitting techniques can derive a continuous representation of continuum kinematics based on finite number of states.

3.1.4. Modal Reduced-Order Model Kinematics

Shape or curvature fitting techniques result in a reduced-order representation of the system state space. The system differential kinematics is interpolated by a continuous curve for which the new state spaces are the curve control parameters (fitting and modal coefficients, control point positions). The fitting curve basis (shape functions) can be the standard basis of a polynomial or Taylor expansion power series,[98,107,120] Lagrange polynomial,[111] Hermite, Bezier, PH, B-Splines, and NURBS curves,[113,125] or Fourier series (i.e., spectral expansion).[108–110,126] Alternatively, for a FEM model, the shape function associated with the dominant deformation modes can be found based on the eigenvalue problem modal analysis of the linearized EoM[121,127–129] or compression analysis via proper orthogonal decomposition method.[130] Modal and fitting techniques result in a continuous (differentiable) kinematic representation, while compression methods result in a discrete but simpler FEM formulation for the system.[130]

The general shape of a continuum rod $g(s)$ is commonly expressed via a polynomial fitting of order n_p as

$$g(s) = \sum_{i=0}^{n_\mathrm{p}} \mathbf{C}_{i(t)}\, s^i \tag{10}$$

where $\mathbf{C}_{i(t)}$ is the time variant coefficient vector (representing system states) and s^i is the polynomial shape (basis) function. Spectral (e.g., Fourier) or power (e.g., Taylor) series and modal approximations of the system kinematics have the same format as Equation (10), except that the time-variant coefficients are replaced by the modal participation coefficients, and the shape function is replaced by the system dominant deformation mode shapes.

The subject of fitting to achieve the reduced-order state space can be either the robot's Cartesian position and orientation (shape fitting) or the strains (strain or, more specifically, curvature fitting). To calculate the system deformation energy, the

position/orientation interpolated relations are differentiated based on an inverse map obtained from Equation (9) as

$$\hat{\mathbf{u}} = R'R^{\mathrm{T}},\ v = R^{\mathrm{T}}\mathbf{p}' - \mathbf{p}'_0 \tag{11}$$

to derive the local linear strains v and curvatures/twist $\mathbf{u}$.[98] In contrast, the strain interpolated relations need to be integrated as in Equation (9) to derive the local position $\mathbf{p}$ matrix representation of rotation R needed for calculating the inertial (e.g., Coriolis forces) and external load actions.

The finite state-space dimension of a modal model is suitable for employing standard rigid-body robotic analysis and control frameworks such as feedback linearization, Jacobian inversion, and load compensation. Shape fitting is favored when constraints (e.g., concentricity), external loads, inertial terms, and control objectives in task space are present, but its integration step involves complex analytical solutions, inaccurate approximations, or implementation of numerical integration schemes. Strain fitting is favored for handling the internal forces (tendon or pressure actuation) and deformation energy where the differentiation steps of the shape fitting method result in computationally expensive relations prone to singularities in inverse formulations. Recent developments in curvature fitting methods for controller design[107] with kinematic constraints[105] emphasize the ever-increasing importance of fitting-based reduced-order techniques in the robotics community. **Table 4** presents a summary of the different implementations of modal techniques to continuum robot kinematics. A future comparative study on the topic, similar to the more general ones in refs. [16,117], would be of significant interest to highlight the advantages and disadvantages of modal approaches in continuum robotics.

3.2. Statics and Dynamics

Traditionally, model-based control strategies for continuum robots favor kinematics over dynamics. Whereas the robot kinematic behavior can be described by simple models (PCC), statics, and dynamics require more complex calculations, resulting in higher computation time,[98] and knowledge of the wrenches on the system, including tendon tension, body weight, and contact reaction forces, as they significantly affect the backbone shape. Such issues resulted in recent developments of simple strategies, such as modal approaches, to incorporate system mechanics in the control framework.[28]

To formulate the statics and dynamics of a continuum robot, different assumptions for the system and material mechanics are considered (see Table 2). The system mechanics can be derived based on the Cosserat rod method,[100] Beam theory,[131,132] PVW,[116,117] and Lagrange method (continuous[104,106,133] or lumped mass[118,134,135]). The material mechanics are usually derived from infinitesimal strain theory[100,133] (Hooke's law) for perfectly elastic material or finite strain theory (e.g., neo-Hookean,[116] Mooney–Rivlin,[136] and Gent[119] methods) and hyper-viscoelastic models (e.g., Kelvin–Voigt method, non-Newtonian fluid viscosity power) in hyperelastic materials.[104] The Cosserat rod theory and Lagrangian/PVW formulations for statics and dynamics are briefly discussed later.

3.2.1. Cosserat Rod Theory Dynamics

A rod with cross-section area a, mass density ρ, and second moment of area j can generally be assumed to be subject to internal forces n, internal moments m, distributed forces $f(\sigma)$, distributed moments $l(\sigma)$, and inertial forces due to acceleration $\ddot{\mathbf{p}}$ (all expressed in global frame) as in Figure 6c.[50] The Cosserat rod equilibrium of an infinitesimal segment of this rod, defined by $\sigma \in [c, s]$ (i.e., with boundaries set by arc-length coordinates c and s), can be expressed as

$$\frac{\partial n}{\partial s} + f(s) = \rho a \ddot{\mathbf{p}} \tag{12}$$

whereas the moment balance is expressed by

$$\frac{\partial m}{\partial s} + \frac{\partial p}{\partial s} \times n(s) + l(s) = j\dot{\omega} \tag{13}$$

Equation (12) and (13) form a boundary value problem with known base configuration and tip loading condition. Numerical integration schemes and nonlinear gradient-based solvers are needed for both the dynamic and static solutions.

Stepping issues due to fast oscillation modes that result in fine temporal integration steps and large deformation modes that result in fine spatial integration steps are the common roadblocks in real-time implementation of Cosserat rod dynamics. Such problems can be avoided by implicitly discretizing the time derivatives in Equation (12) and (13) and solving the resulting boundary value problem in arc length s at each time step.[102,137] The integration of the Cosserat rod method in a controller design framework is not straightforward, but possible through an optimization for the system inverse mechanics[101] or with continuous system control theories.

Table 4. Reduced-order kinematics for continuum robots.

Categories	EoM	Shape function	States	References
Compression techniques	Discrete	Proper orthogonal decomposition	Element deformation and velocities	[127–130,151]
Modal and standard fitting techniques	Continuous ODE	Spectral (e.g., Fourier)	Modal participation coefficients	[108–110,126]
		Power series (e.g., Taylor)	Polynomial coefficients	[98,107,120]
		Shape fitting	Control point positions	[111]
			Fitting method parameters (e.g., point, local slope)	[113,125]

3.2.2. Lagrangian and TMT Dynamics

Discrete and modal kinematics simplifies a continuum system to an equivalent finite-state series of rigid or compliant counterparts. The dynamics of such systems can be produced via derivation of the system Lagrangian (based on the elements' kinetic and potential energy[118,133]), PVW (based on the elements' virtual displacement[104]), or a recursive computational scheme[133] (also called inverse Newton–Euler algorithm, inverse dynamic model, or reduced-order integration[99,138]). A continuous representation of the system Lagrangian can be employed for the case of reduced-order modeling.[105]

The alternative TMT method, owing its acronym to the $T^{\mathrm{T}}MT$ formulation of the projected inertial term M onto the state space using the space transformation Jacobian T, derives system dynamics in a vector formalism based on PVW with fewer derivation steps compared to the Lagrangian method.[98,111,112] The resulting finite-state system is computationally lighter than Cosserat rod dynamics, and compatible with rigid-body nonlinear control design techniques. However, the EoM are less accurate due to the underlying approximated kinematics, time stepping issues, and complex derivations prone to numerical instabilities. FEM and fitting may solve instability in such a framework.[98]

3.3. Complementary Modeling Considerations

3.3.1. Tendon Routing Friction

Trying to understand the effect of tendon routing friction on the shape of continuum robots has driven the efforts of several research groups, which modeled the tendon–vertebra interaction in specific robot designs.[139] Even if those works proved that friction influences the robot's shape and modeled it with good accuracy (error in the order of 5% of robot length[140]), they are limited by simplifications and lumped parameters, while in general being challenging to implement.

3.3.2. Cross-Section Deformation

A similar behavior is caused by cross-section deformation of hyper-elastic parts. Cross-section deformation modeling is critical for braided extensors or McKibben actuators,[100] where the relation between the material fundamental stretch values is derived on the assumption of incompressibility (constant volume) and the braid's constant length constraints to compute the hyper-elastic material deformation energy. PVW is the preferred choice for incorporating this effect in the EoM. The same method can be used for the exact modeling of a cross section under deformation showing a 6–8% increase in accuracy for a pneumatic silicon appendage.[116,117]

3.3.3. System Stability

Specific classes of continuum robots, such as concentric tube robots, feature bistable or unstable structural configurations. The multiplicity of stable solutions and sensitivity of the models to external perturbances and modeling errors close to such unstable configurations might affect numerical convergence and degrade model accuracy. To avoid unstable phenomena through design and control, stability limits can be modeled with approaches such as the system's linearized governing equations,[51] investigating the momentum-free condition at the robot tip,[141] and elastic stability theory.[142]

3.3.4. Solution Strategies

A continuum robot model results in a system of nonlinear algebraic equations (in the case of discrete kinematic and static models), an ordinary differential equation (ODE, for modal and discrete dynamic models) or PDEs (for modal static and Cosserat rod models). Direct forward integration schemes (e.g., Runge–Kutta) can be used for ODEs in the absence of loads,[119] or in a general case with known base wrench[143,144] or dynamic derivation based on discretized kinematics (e.g., PCC[98,120]). Otherwise, a root finding or a boundary value problem will be formed to be solved by an indirect numerical scheme such as shooting[100–102,116] (relying on Jacobian-based numerical optimization), FEM solvers,[145–148] or Ritz[106,109,114,149] and Ritz–Galerkin[111,150,151] methods.

3.3.5. Software Frameworks

Developing software frameworks for modeling and control of continuum robots is receiving increased attention to address the needs of the growing multidisciplinary continuum robotic research community.[152] **Table 5** collects the main recently developed software packages.[153–159]

3.3.6. Learning-Based (Model-Less) Methods

Engineered systems exhibit backlash, friction, and hysteresis. In addition, fabrication inconsistences and inherent modeling assumptions lead to errors in models. Numerical simulations[160] and experimental calibration[161] have been considered to address these issues. Recent efforts try to experimentally identify the kinematics or the dynamics of the robot, rather than modeling the robot beforehand. Collected data are used to train neural networks[162–164] and, more recently, Koopman operator

Table 5. Software packages for continuum robotics research.

Name	Platform (language)	Theory	References
SOFA	C++ & Python	FEM mesh	[121]
PyElastica	Python	Discretized Cosserat	[103,153]
ChainQueen	C++ & Python	FEM mesh	[154]
SimSOFT	C++	Discretized Cosserat	[124]
TMTDyn	MATLAB	PCC, ROM, lumped mass, FEM (mesh)	[98]
IPC	C++	FEM mesh	[155]
SoMo	Python	Lumped mass	[156]
AMBF	C++ & Python	FEM mesh	[145,157]
SoftIK	C++	FEM mesh	[158]
SoRoSim	MATLAB	PCC/PVS	[159]

frameworks[165] to predict robot behavior in seen and unseen configurations. These model-less approaches can potentially achieve high accuracy and even reliable full shape reconstruction. However, their performance is reliant on the quality of the dataset, and the results are only valid for the specific robot for which data was collected. For detailed review of learning-based methods, the reader can refer to recent articles on modeling and control.[26–31]

4. Sensing, Control, and Planning

The unique structure of continuum robots requires sensing solutions, control methods, user interfaces, and navigation strategies that are fundamentally different from the ones of rigid-link robots. In this section, we discuss these solutions with reference to practical examples.

4.1. Sensing

Measuring the infinite DoFs of continuum robots is challenging, and distributed sensors are needed for an accurate shape estimation. Given the tight design constraints and the extrinsic actuation of many continuum robots, sensor design and placement need to be tailored to the specific structure and not hinder motion. These constraints have led to the development of a variety of proprioceptive (i.e., measuring the robot's state) and exteroceptive (i.e., measuring the interaction with the environment) sensing methods.[32,33,166]

4.1.1. Proprioception: Shape Sensing

The shape of the backbone can be measured through multiple principles. State-of-the-art commercial technologies include the following:

Motion Capture: Motion capture systems can be extremely accurate,[167,168] but require an unobstructed field of view that is rarely available in the narrow geometries where continuum robots operate. While they can be integrated with the robot's software, they are placed externally of the robot's body and "core" hardware.

Endoscopic Cameras: Onboard cameras are usually employed as exteroceptive sensors, but can also provide a limited measure of the robot's state.[169,170]

Electromagnetic Trackers: Electromagnetic sensors have been successful in applications with limited interference from the environment, such as surgery.[171,172]

Fiber Bragg Grating (FBG): FBG sensors can measure bending with high accuracy, but are limited by their complex and expensive manufacturing process and high sensitivity to twist.[173–177]

Less common methods, demonstrated on prototypes but with limited availability on the market, include the following:

Hall Effect: The combination of NdFeB magnets and Hall elements on a flexible circuit can be used to measure curvature (up to 0.035 mm^{-1}[178]) with a fast response.

Inductance Sensing: By measuring the change in mutual inductance between coils on joints, joint orientation can be measured with an accuracy of 1.1°.[59]

Optoelectronics: Stretchable optical waveguides and optical transducers have been used for strain sensing with low hysteresis and high precision.[179,180]

Piezoelectric Polymers: PVDF sensors can track the shape changes of hyper-flexible beams, even if they have been demonstrated mainly for 2D applications.[181]

Stretch Sensors: Stretchable elongation sensors (either resistive or capacitive with ionic liquids) can be included along the robot's backbone for indirect shape measurement through a kinematic mapping.[182]

4.1.2. Exteroception: Contact and Force Sensing

When conventional force or pressure sensors are constrained by space limitations, sensing skins based on stretchable capacitive or resistive strain sensors can be installed on the body surface of continuum robots to directly measure reaction forces due to contact with the environment.[183–186]

Model-based force-sensing methods can reconstruct the loading configuration of a continuum robot from its shape or actuation. Shape-based force sensing through backbone shape can be achieved with a probabilistic approach,[187] with a kinetostatic model,[188] or by measuring the shape through images[189] or electromagnetic sensors.[190,191]

Actuation-based approaches that use joint-level information are also addressed as intrinsic force sensing. Intrinsic force sensing is often obtained with the PVW, with a PCC formulation[192–194] (which can be extended into a framework for hybrid force/position control[195,196] or the Cosserat rod theory kinetostatic modeling.[37] Specific solutions can also be used to achieve direct force sensing, such as the pneumatic cylinders,[197] strain measurements from FBG sensors,[198–200] or tactile arrays.[201]

4.2. Control Methods

When compared to their rigid-link counterparts, continuum robot controllers face additional challenges such as virtually infinite-DoF motion, non–linear material properties[202,203] (e.g., hysteresis), and prototypical technologies with a wide range of unique solutions, hindering the development of a unified control framework.[27] Existing control methods can be classified according to their modeling approach: model-based controllers,[28] model-free controllers with data-driven techniques (e.g., machine learning and empirical methods), and hybrid controllers that combine both solutions.

In model-based control, up to three kinematic models link the robot's four operating spaces: actuation (monitored with encoders and wrench sensors), joint (e.g., tendon length), configuration (e.g., shape parameters), and task space (i.e., Cartesian position and orientation of the end-effector). As such, low-level controllers can be implemented in "lower" layers to track and compensate for actuator/joint-related errors (e.g., cable friction, tendon coupling, hysteresis), while configuration and task space controllers act directly on the robot's motion target, providing robustness to model uncertainties. However, actuator/joint space controllers are more stable and allow for higher frequencies (with a better dynamic performance).[27]

Conversely, model-free approaches are independent of joint and configuration parameters and can provide a robust and stable performance when model-based approaches falter (e.g., highly nonlinear systems, unstructured environments).[31] However, model-based controllers are more reliable and favored in critical applications such as surgery. To merge the advantages of both solutions, hybrid techniques can integrate model-based and model-free approaches at different kinematic layers[27] or use models to drive learning.[28]

4.3. Teleoperation

Since continuum robots often operate in critical conditions, such as surgery or radioactive environments, remotely controlled operation is favored. As such, control interfaces are a key part of continuum systems. A standard graphical user interface can support the visualization of the environment, but enhanced teleoperation with haptic feedback is preferred. Force data improve transparency in precise manipulation through kinesthetic (force) and cutaneous (tactile) feedback,[204] but haptics depends on the quality of force sensing in the remote environment, achieved as explained in Section 4.1.

Moreover, teleoperation is hindered by the dissimilarity between the physical interface (i.e., leader device, usually a rigid mechanism) and the continuum follower. This problem can be addressed with hardware solutions, such as joysticks with tailored mapping,[205] rigid-link leaders,[206,207] commercial haptic devices,[37,208] and continuum interfaces that avoid kinematic dissimilarity.[209–211]

4.4. Motion Planning

While path planning strategies from rigid robots can be adapted to continuum robots, three unique motion patterns take advantage of their inherent slenderness and flexibility: follow the leader (FTL), circumnutation, and coiling.[212–214] These patterns allow continuum robots to navigate narrow and confined spaces that cannot be accessed by other systems and exploit environmental features to increase performance.[196–198]

4.4.1. Follow the Leader

FTL motion requires the robot's shape to conform along the path led by its tip (**Figure 7**a,b),[215] with key applications in surgery

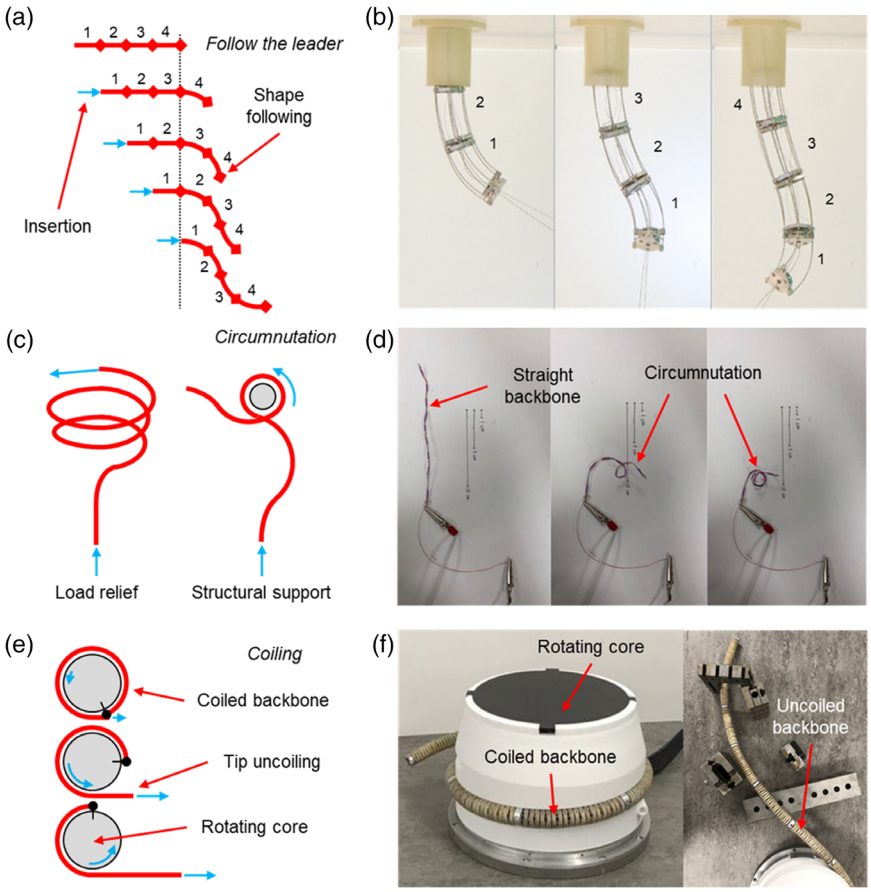

Figure 7. Motion strategies for continuum robots: an example of follow-the-leader (FTL) motion for a) a multi-segment continuum robot and b) a prototype with intrinsic tip-following capabilities; Reproduced under the terms of a CC BY license.[220] Copyright 2016, The Authors, published by PLOS. c) circumnutation for load relief or additional structural support generation and d) an shape-memory alloy (SMA)-based continuum robot example; Reproduced under the terms of a CC BY license.[236] Copyright 2020, The Authors, published by Frontiers Media. e) a schematic representation of coiling, f) with an example of a coiled and uncoiled continuum robot for nuclear applications.[240]

thanks to minimal invasiveness. During robot insertion in the workspace, the exposed length of the robot gradually increases as the tip advances. However, to navigate around obstacles, the shape of the backbone must be constant over time. Thus, the robot's body must follow the path of its tip.

With reference to the Cosserat model in Section 3, the backbone shape during robot insertion can be described with a time-varying arc-length parametrized transformation $g(s,t) \in \mathrm{SE}(3)$, with centerline position $\mathbf{p}(s,t) \in \mathbb{R}^3$ and orientation $R(s,t) \in \mathrm{SO}(3)$ with respect to arc length $s \in [0, \ell(t)]$. The time-dependent length function $\ell(t)$ represents the exposed length of the robot, which is the length of the robot that has been inserted in the workspace, rather than the full length of the body as described in previous sections. The evolution of the path of the continuum robot $\mathbf{p}(s,t)$ can be expressed as

$$\mathbf{p}'(s,t) = \frac{\partial \mathbf{p}}{\partial s} = z(s,t) \tag{14}$$

when the z-axis $z(s,t)$ of $R(s,t)$ is tangent to the curve. We can assume that rotation and position are fixed at insertion point $s = 0$ as $R(0,t) = R_z(\varphi_0(t))$ and $\mathbf{p}(0,t) = 0$ Respectively. When using an FTL approach, the position at any arc length of the curve does not change in time.[216] This condition can be expressed as

$$\dot{\mathbf{p}}(s,t) = \frac{\partial \mathbf{p}(s,t)}{\partial t} = 0 \tag{15}$$

where the dot denotes a partial derivative with respect to time.

However, some continuum robots, such as the ones with a segmented backbone, cannot conform to the condition in Equation (15). In those cases, only an approximation of this ideal motion can be achieved by minimizing the displacement of backbone shape between consecutive poses defined by $\mathbf{p}(s,t)$, and $\mathbf{p}(s,t+\Delta t)$ following a change in exposed length $\Delta\ell$, as

$$\min(\mathbf{p}(s,t+\Delta t) - \mathbf{p}(s,t)) \tag{16}$$

This optimization is performed along the exposed length ℓ shared by the two poses, denoted by $s \in [0, \ell(t)]$ during insertion and $s \in [0, \ell(t+\Delta t)]$ during retraction.

Examples of FTL motion in segmented continuum robots are reported in refs. [217–219]. Specific tendon-driven designs have also been developed to intrinsically FTL by adding extension capabilities.[220–222] With concentric tubes, specific deployment sequences and tube pre-curvature help minimize the deviation from exact FTL motion.[216,223–225] Soft growing robots also intrinsically FTL through eversion.

4.4.2. Circumnutation

Circumnutation is a phenomenon that can be observed in plants' vines[226] and roots,[227] presenting the elliptical and spiral trajectories in Figure 7c.[227,228] Despite the many qualitative and quantitative studies on this oscillatory rotational motion,[228] the reason and scope of circumnutation is not yet fully understood, but this motion pattern seems to have a significant influence on reducing resistance in soil penetration and relieving external loads in the air.[229] Thus, an advantage of this motion is a reduced force on the backbone of a robot that penetrates a viscous environment such as artificial soil,[230] especially when combined with growth.[231]

Circumnutation also increases the probability of efficient contact with supports in open environments.[232] When suspended, thin and long continuum bodies usually lack structural support and struggle with buckling and sagging even without external loads. Plants' vines have a similar structure but grow by sequentially bending in different directions. In this way, plants are more likely to find support in an unstructured environment and partially decouple distal loads.

As shown in Figure 7c, this strategy can be applied to continuum robots with spring-loaded concentric tube design to initiate environmental contact via growing central backbones and artificial prickles.[228,229] Furthermore, the interaction with the environment during circumnutation has been investigated in refs. [233–235], where modeling approaches are presented to predict growth trajectories through holes and against obstacles for open-loop control.

4.4.3. Coiling

Bioinspiration is at the core of many recent continuum robot designs and motion strategies.[232] Snakes coil to defend themselves, as being stretched out leaves them vulnerable to predators. A coiling motion can be observed in plants that curl their stems around supporting features to increase load-bearing capacity (as part of circumnutation). A coiling continuum robot facilitates both storage and deployment through a smaller form factor, as well as improves performance with circumnutation.

Passive or semi-active coiling can be achieved by SMA[236] and air muscles.[237] Wrapping motion[238] and tendril-based grasping have also been studied for manipulation.[239] Further, an active FTL uncoiling enables robot deployment in narrow spaces and improves navigation (Figure 7f).[240] Active coiling can be achieved by computing an optimal trajectory that minimizes displacement from the desired one.[241]

5. Applications

In evaluating current and potential applications of continuum robots, it is useful to consider the capabilities of these structures in comparison to traditional (i.e., rigid-link) robots. The two types are in some sense "dual". Rigid-link structures offer relatively high precision and load capacity, at the cost (and because) of the rigidity of their structures. Continuum structures are compliant and maneuverable, at the cost of relatively lower precision and load capacity. Since the early days of robotics, rigid-link manipulators have been successfully applied to high-precision applications where environmental changes are not significant (e.g., engineered/factory environments). These can be viewed as "natural" applications for rigid-link robots.

For continuum robots, "natural" applications can be projected to be those requiring higher adaptability to the environment. In particular, the ability of continuum structures to deploy their narrow profiles in tight and congested environments enables application areas beyond the scope of traditional robots. One highly successful such "natural" application area for continuum robots has been inside the human body, in various medical procedures.

Table 6. Continuum robot applications.

Application	Environment	Example tasks	Size[a)]	Key requirements
Medicine	Human body	Inspection[34–36] Surgery[34–36]	Diameter: 2–20 mm Length: up to 1.5 m	Human patient safety
Aerospace	Aeroengine Space station	Repair (machining,[242] laser,[46] flame[243]) Inspection[10,229,241]	Diameter: 6–15 mm Length: up to 5 m	Process dynamics Heat resistance (aircraft) Works in 0 gravity (space)
Water	Maritime vehicles	Active hose (fuel)[246]	Diameter: 40 mm Length: 1 m	Dynamic position control
Construction	Construction sites	Active hose (cement)[247]	Diameter: 15 mm Length: 1 m	High internal pressure
Nuclear	Glovebox Storage tanks	Decommissioning[240,248] Active hose (air)[251]	Diameter: 15 mm or more Length: up to 16 m	Works with radioactivity Robot decontamination
Search and rescue	Underground Harsh terrain	Exploration and mapping[9,65,249] Active hose (water)[245,249]	Diameter: 10–50 mm Length: up to 20 m	Protection from possible environmental hazards
Manipulation	Varies	Manipulator arm[61] Soft fingers[254–257]	Varies	Grasping force High payload

[a)]The reported size represents a general indication. The actual values for specific applications may vary.

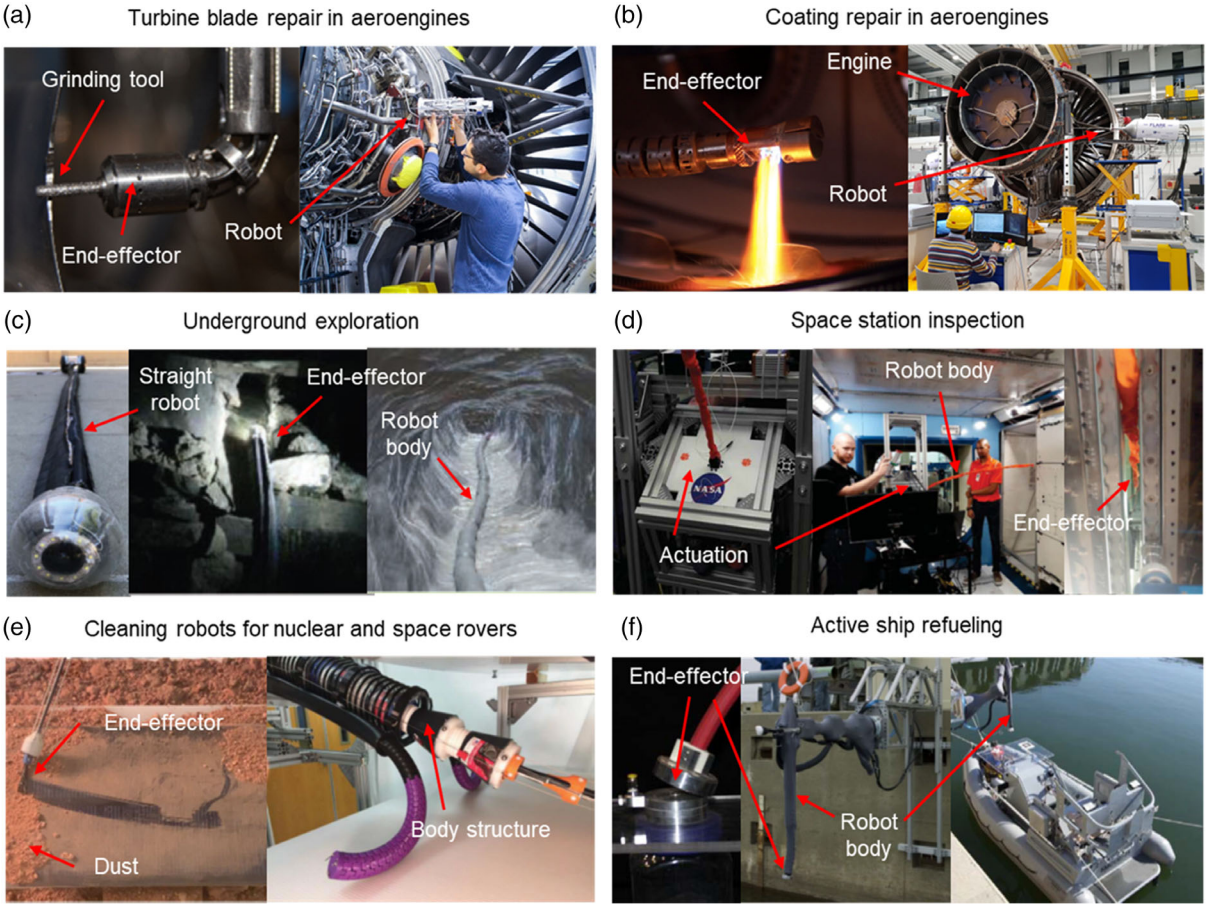

Figure 8. Examples of industrial applications of continuum robots: inspection and repair of aeroengines, a) with examples of blade repair; Reproduced with permission.[242] Copyright 2021, Elsevier; and b) coating repair; Reproduced with permission.[243] Copyright 2022, IEEE; c) exploration of underground tunnels; Reproduced with permission.[249] Copyright 2020, IEEE; d) inspection of hard-to-reach areas of a space station; Reproduced with permission.[229] Copyright 2018, IEEE; e) dust cleaning on a solar panel; Reproduced with permission.[250] Copyright 2020, IEEE; and in a nuclear glove box; Reproduced with permission.[251] Copyright 2019, IEEE; f) active hose for ship-to-ship refueling. Reproduced with permission.[246] Copyright 2015, IEEE.

As extensive reviews for this particular application exist,[34,35] we focus here on other emerging applications, summarized in **Table 6**.

5.1. Inspection and Repair for Aerospace

The ability of slender continuum structures to penetrate and navigate congested environments, effectively operating as active borescopes, is enabling applications in aerospace. Notably, a long-term collaboration between industry and academia has resulted in the development of slender continuum robots for aeroengine repair.[10,45,46] In a first industrial demonstration for aerospace, a 24-DoF 1.2 m long continuum robot (15 mm diameter at the tip) with two cameras and exchangeable grinding tools at the tip accessed an aeroengine from the front to inspect and repair low-pressure compressors.[10] A 5-DoF continuum robot was demonstrated in teleoperated aerofoil repair, which enables a fast response to fleet repair needs around the world thanks to a specialist operating remotely (**Figure 8**a).[242] Multiple continuum arms were also used for collaborative operations in aeroengines. Two 0.7 m long continuum robots achieved thermal barrier coating repair of a commercial aeroengine combustor through narrow inspection holes. These two arms separately manipulated an extreme temperature flame (3000 °C) for repair and cameras/support tools (Figure 8b).[243] Finally, a 5 m long continuum robot (9.1 mm diameter) has been demonstrated for long-reach inspection and maintenance in aeroengines.[244]

Another potential application for thin continuum robots is for in-space inspection. Specifically, the work in ref.[229] describes the development and of a continuum robot for inspection in between and inside equipment racks in the International Space Station (ISS). Testing in a full-scale mock-up of the Space Station at NASA is described (Figure 8d). Further applications supporting exploration on planetary bodies are projected.

5.2. Active Hose for Fluid Delivery

Another natural use of continuum robots is as "active hoses", across a variety of applications. The interior of the backbone of continuum structures provides a direct path for (application-specific) fluids to be pumped through the backbone, while taking advantage of the ability to actively shape the path. First discussed in ref. [245], the concept of active robot hoses has been the subject of increased interest recently, as several groups have explored a variety of potential applications. The potential of continuum robot hoses to transfer fuel in ship-to-ship refueling operations was explored in ref. [246]. Successful proof of concept experiments in shore-to-ship refueling were reported (Figure 8f).

More recent work is aimed at the construction industry, via additive manufacturing (3D printing) of cement.[247] In this application, the maneuverability of the continuum backbone (physically, an industrial cement hose retrofitted with a cable harness for remote tendon actuation) provides better access in congested construction sites, and allows more dexterous (i.e., beyond vertical) positioning of the nozzle to build and repair complex structures. For any additive manufacturing process, continuum robots could significantly increase nozzle dexterity to enable the fabrication of complex shapes and geometries and remove the need for support material.

The pumping of water through continuum structures is reported in ref. [248] for high-pressure cleaning, and in ref.[249] with projected applications in suppressing fires. Other works have demonstrated active continuum hoses pumping air, for example in ref. [250], where the focus was on a space application, aimed at cleaning dust from solar panels on planetary rovers (Figure 8e).

These potential applications, together with the exponential growth of additive manufacturing technologies, are expected to further increase interest in continuum robots as active hoses.

5.3. Operation in Hazardous Environments

As with rigid-link robots, continuum robots have found application in remote and dangerous applications. The need to operate in congested, highly radioactive environments provided the motivation for one of the earliest (and largest: 16 m length, 18 000 kg mass) applications of continuum robots.[248] More recent efforts[240,251] also aimed at the nuclear industry have proposed the deployment of continuum robots in contaminated glove boxes (Figure 8e). However, operation in radioactive environment exposes the robot to contamination: unless a solution for cleaning or preventing contamination is developed, only disposable robots can be employed in these applications.

Search and rescue operations are characterized by different kinds of hazards, such as abandoned or collapsed infrastructures or fires. In these scenarios, soft growing robots have been proposed to enable exploration, mapping, and intervention thanks to their reach in unstructured environments.[249,252]

It can be anticipated that further applications for continuum robots in remote and dangerous environments (e.g., undersea, military) will emerge in the next few years.

5.4. Manipulation

The flexible backbone of continuum robots can conform to objects of any shape, enabling a "gentle" grasp on easy-to-damage items (e.g., fruit and vegetables), or items with complex geometries.[253] From continuum manipulators[61] to hands and grippers with continuum fingers,[254,255] this topic has been first discussed in the rich literature on soft robotics[11,12,14] and recently subject to systematic studies to obtain a grasp taxonomy for the synthesis and control of grasping operations with continuum robots,[256,257] which are likely to lead to new designs and applications in future developments.

6. Open Challenges

Despite the substantial body of work and progress reviewed herein, continuum robots as a field remains in its early stages. Many substantial questions and issues remain open. In this section, we review key open challenges, summarized in **Figure 9**.

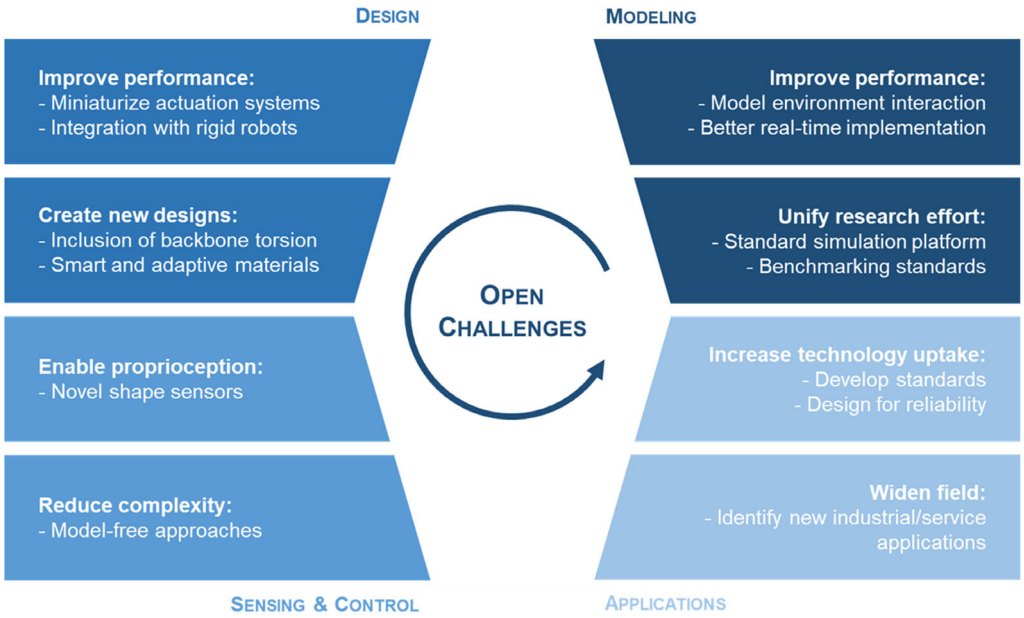

Figure 9. Open challenges.

6.1. Design

Currently, there are several well-established design options (e.g., concentric tubes, remote tendon actuation, local artificial muscle actuation) for realizing continuum robot hardware. However, further innovative and/or fundamentally new design concepts for realization and refinement of continuum robot backbone structures is strongly motivated. Current designs lack some of the key features which make the biological structures that inspire them so effective. For example, efforts to reproduce torsion about the backbone (key to the operation of octopus arms and elephant trunks) and to incorporate artificial suckers (the dexterity-enhancing "fingers" for the backbone "arm" of the octopus) remain at a preliminary stage. The inherently modular growth and hydraulic actuation of plant stems and structures is motivational for the field, but transformation of those concepts into continuum robot hardware remains elusive.

Advances in smart and adaptive materials and novel manufacturing processes may enable new related opportunities in continuum robot design, but the pathway for this remains largely unexplored. Note that an underlying hardware challenge is that—particularly at the small scale—physical space in the backbone for the addition of enhanced capabilities is severely limited, inherently restricting what can be achieved.

The deployment of externally actuated continuum robots is hindered by bulky actuation units and linear stages to "feed" the robot into the workspace. Extrinsic actuation is also limited by transmission efficiency, as part of the motor wrench is lost to friction and other factors. While this loss is limited at small scales, large-scale applications with extrinsic actuation (e.g., slender designs with an extremely long reach but a reduced diameter) are impacted by this issue, which also affects their accuracy. These issues can be addressed by developing more compact and portable actuation technologies, or by miniaturizing intrinsic actuation. This would directly benefit large-scale continuum robots, as onboard actuation causes undesired deflections and reduces payload.

A more general open question relates to how continuum robots should be utilized and integrated into more general systems. Should their ultimate niche be as manipulator arms, and/or as locomotion platforms? Continuum robots can be viewed as existing in the space between well-established "hard-bodied" manipulators and the rapidly emerging area of soft robots. We speculate that "hybrid" rigid/continuum/soft structures are likely to be the future of robotic hardware. However, how to realize such hybrid robots, to take advantage of the strengths of each type while compensating for their weaknesses, will be a significant and interesting challenge.

6.2. Modeling

As discussed earlier in this review, much attention has already been paid to developing models of various types for continuum robots. Continuum robot structures offer a rich underlying arena for study, with not only techniques used in modeling "traditional" robots, but additionally other "non-traditional" areas, for example, continuum mechanics, applicable. However, much of this potential remains to be understood and explored, and many existing models can benefit from refinement. For example, a formal theory for grasping with continuum structures, analogous to that established for multi-fingered robots, is currently lacking. Furthermore, although continuum robot kinematics is well understood and dynamics currently an active research area, few works incorporate models of environmental interaction and/or dynamic contact. Careful consideration also must be made of the tradeoffs between accuracy and computational complexity in current modeling approaches.

Models are required for simulation as well as real-time implementation. Generalizable and graphical simulation of continuum robots are relatively underdeveloped areas, complicated by the uncertainty inherent in existing models, and the fact that few existing models consider environmental contact, a desirable

aspect in graphical simulation. The lack of a common simulation platform to demonstrate and share algorithms hinders research in the field. Currently, most research groups simulating continuum robots develop one-of-a-kind code suites customized to their own research specialty. A public domain, open-source graphical simulation environment which could be expanded to incorporate alternative and emerging models would be a valuable and welcome addition and resource to the research community.

6.3. Sensing

Endowing continuum robot hardware with sensing has been, and remains, a major issue for both proprioception, which refers to the robot's ability to sense its own motion, location, and action, and exteroception, which is the robot's perception of the external environment. For external sensing of the environment, there is often strong motivation to include the associated sensory systems within the continuum body, since many projected applications are in tight and congested spaces (to take advantage of the maneuverability of the continuum structure), making it hard to use externally located sensor systems. However, it can be a significant challenge to embed, power, and interface with sensors given the limited space in the backbone. Similar issues of available space apply to internal sensing of backbone shape (configuration). Solutions which infer shape from quantities sensed at the base on the robot (tendon lengths, tensions, etc.) are limited in effectiveness by the compliance of continuum hardware (e.g., external forces can change the backbone shape without altering tendon lengths). Potential alternative and emerging solutions for backbone shape sensing which appear attractive include fiber optics, which can be directly integrated into the backbone structure. However, new and alternative technologies and strategies are highly desirable.

6.4. Control

Practical implementation of continuum robots is closely linked to issues arising from complexity and uncertainty in their modeling. Real-time computation of some model-based algorithms can be challenging at best, and the inherent uncertainty in models places an increased burden on controllers. While a variety of approaches to controller development for continuum robots have been suggested and evaluated, the field remains a long way from a consensus on the best approach. An intriguing open issue is the tradeoff between model-based and learning-based approaches to real-time continuum robot motion planning and control. Learning-based approaches offer adaptability and computational efficiency at the cost of loss of generalizability. It appears likely that, in the near future, greater emphasis will be placed on model-free learning-based approaches, or combinations of model-based and learning-based approaches, to problems of motion planning and control of continuum robots.

6.5. Applications

Finally—and arguably most importantly—new and wider applications for continuum robots are needed for the area to continue to thrive and grow. Applications in medicine nurtured the nascent field and remain predominant in practical continuum robot deployment. Medicine is thus currently, and is likely to remain, a key focus of interest and research in the area. However, industrial interest is growing, as continuum robots are uniquely suited to on-site inspection, maintenance, and repair tasks on key infrastructures precluded to conventional robots, such as turbine engines, underground ducts, power plants, and rescue sites (e.g., a collapsed building).

The application focus is thus widening, as discussed and reviewed herein. To stimulate both ideas and research and to grow the field to match its potential, the identification and pursuit of new, unique, and useful applications for continuum robots must surely be a necessary catalyst.

Appendix:

Methodology

Our search methodology involved a literature search using keywords (e.g., "continuum robots", "concentric tube robots", "soft

Table A1. Glossary.

Term	Abbreviation	Description
Absolute nodal coordinate formulation	ANCF	FEM-like modeling techniques that divides the body of the robot in many discrete nodes
Backbone	–	Core element of a continuum robot, defining the centerline of its body
Circumnutation	–	Motion mode typical of plants; consists of coiling motes to increase payload
Concentric tube robot	–	Design with pre-curved tubes nested into each other
Configuration	–	Position and orientation along the backbone curve
Curvature	–	Amount by which a curve deviates from a straight line, defined as the reciprocal of the curve's bending radius
Degree of freedom	DoF	–
Equation of motion	EoM	–
Extrinsic	–	Referring to actuation or sensors located externally
Fiber Bragg grating	FBG	Fiber-based shape sensing technique
Finite-element method	FEM	Modeling technique that divides the body of the robot in many discrete elements
Fluid muscle robot	–	Design actuated intrinsically with pressurized fluid
Follow the leader	FTL	Motion strategy in which the robot's shape conforms along the tip path
Intrinsic	–	Referring to actuation or sensors distributed along the backbone of the robot
Ordinary differential equations	ODEs	–
Partial differential equations	PDEs	–
Piecewise constant curvature	PCC	Modeling technique that approximates the backbone curve with circle arcs

Table A1. Continued.

Term	Abbreviation	Description
Piecewise constant strain	PCS	Modeling technique that approximates the backbone curve with constant strain curve segments
Principle of virtual work	PVW	–
Pseudo rigid body	PRB	Modeling technique that approximates the backbone with a highly articulated rigid chain
Reduced-order model	ROM	Modal modeling technique
Rod-driven	–	Actuated by pulling and pushing rods along the backbone
Shape	–	Position and orientation along the backbone curve
Shape-memory alloy	SMA	Smart material that changes shape when heated
Soft growing robot	–	Design able of a significant backbone length increase
Tendon driven	–	Actuated by pulling and releasing tendons along the backbone
Twin pivot	–	Design with two flexible elements in parallel, constraining bending to a single direction
Variable curvature	VC	Continuous modeling technique
Vertebra	–	Rigid element along the backbone for tendon routing

robots") in flagship robotics journals (e.g., Robotics Q1/Q2 journals in Clarivate's Journal Citation Report), conferences (e.g., ICRA, IROS, RoboSoft), and databases (SCOPUS, Web of Science, IEEE Xplore), for a total of over 12 000 matching papers.

The search results were first analyzed to identify the key literature surveys on the topic, listed in **Table A1**. These surveys have been used for up to two steps of backward (i.e., examining their bibliographies) and forward (i.e., tracking papers that have referenced those surveys on SCOPUS and Google Scholar) citation tracing to detect key references missed by the keyword search. Further studies were added by the authors from their knowledge.

After removing duplicate studies, the bibliography was obtained by selecting references by number of citations (for older papers) and relevance of the content to the scope of this survey, prioritizing recent works and nonmedical applications.

Conflict of Interest

The authors declare no conflict of interest.

Keywords

continuum robots, control, design, modeling, robotics, soft robots

Received: October 19, 2022
Revised: February 7, 2023
Published online: March 23, 2023

[1] I. D. Walker, H. Choset, G. S. Chirikjian, *Springer Handbook of Robotics*, Springer, Cham **2016**, pp. 481–498.
[2] V. C. Anderson, R. C. Horn, *Mech. Eng.* **1967**, *89*, 54.
[3] G. Robinson, J. B. C. Davies, in *Proc. IEEE Int. Conf. Robotics and Automation*, IEEE, Piscataway, NJ **1999**, pp. 2849–2854.
[4] R. Cieslak, A. Morecki, *Robotica* **1999**, *17*, 11.
[5] G. Immega, K. Antonelli, in *Proc. IEEE Int. Conf. Robotics and Automation*, Nagoya, Japan **1995**, pp. 3149–3154.
[6] K. Suzumori, S. Iikura, H. Tanaka, in *Proc. IEEE Int. Conf. Robotics and Automation*, Sacramento, CA **1991**, pp. 1622–1627.
[7] N. Simaan, R. Taylor, P. Flint, in *Proc. IEEE Int. Conf. Robotics and Automation*, New Orleans **2004**, pp. 351–357.
[8] A. Degani, H. Choset, A. Wolf, M. Zenati, in *Proc. IEEE Int. Conf. Robotics and Automation*, Orlando, FL **2006**, pp. 4167–4172.
[9] J. D. Greer, T. K. Morimoto, A. M. Okamura, E. W. Hawkes, *Soft Rob.* **2019**, *6*, 95.
[10] X. Dong, D. Axinte, D. Palmer, S. Cobos, M. Raffles, A. Rabani, J. Kell, *Rob. Comput. Integr. Manuf.* **2017**, *44*, 218.
[11] D. Trivedi, C. D. Rahn, W. M. Kier, I. D. Walker, *Appl. Bionics Biomech.* **2008**, *5*, 99.
[12] S. Kim, C. Laschi, B. Trimmer, *Trends Biotechnol.* **2013**, *31*, 287.
[13] I. D. Walker, *ISRN Rob.* **2013**, *2013*, article no. 726506.
[14] C. Laschi, B. Mazzolai, M. Cianchetti, *Sci. Rob.* **2016**, *1*, eaah3690.
[15] Z. Li, L. Wu, H. Ren, H. Yu, *Mech. Mach. Theory* **2017**, *107*, 148.
[16] P. Rao, Q. Peyron, S. Lilge, J. Burgner-Kahrs, *Front. Rob. AI* **2021**, *7*, 223.
[17] F. Janabi-Sharifi, A. Jalali, I. D. Walker, *IEEE Access* **2021**, *9*, 68703.
[18] S. Li, G. Hao, *Actuators* **2021**, *10*, 145.
[19] H. B. Gilbert, D. C. Rucker, R. J. Webster III, *Rob. Res.* **2016**, 253.
[20] A. W. Mahoney, H. B. Gilbert, R. J. Webster, *The Encyclopedia of Medical Robotics*, World Scientific, Singapore **2018**, pp. 181–202.
[21] H. Alfalahi, F. Renda, C. Stefanini, *IEEE Trans. Med. Rob. Bionics* **2020**, *2*, 410.
[22] Z. Mitros, S. M. H. Sadati, R. Henry, L. Da Cruz, C. Bergeles, *Annu. Rev. Control Rob. Auton. Syst.* **2021**, *5*, 335.
[23] M. Manti, V. Cacucciolo, M. Cianchetti, *IEEE Rob. Autom. Mag.* **2016**, *23*, 93.
[24] Y. Yang, Y. Li, Y. Chen, *Bio-Des. Manuf.* **2018**, *1*, 14.
[25] R. J. Webster III, B. A. Jones, *Int. J. Rob. Res.* **2010**, *29*, 1661.
[26] H. B. Gilbert, *Front. Rob. AI* **2021**, *8*, 732643.
[27] T. G. Thuruthel, Y. Ansari, E. Falotico, C. Laschi, *Soft Rob.* **2018**, *5*, 149.
[28] C. Della Santina, C. Duriez, D. Rus, arXiv preprint arXiv:2110.01358, **2021**.
[29] C. Armanini, F. Boyer, A. T. Mathew, C. Duriez, F. Renda, *IEEE Trans. Rob.* **2023**, https://doi.org/10.1109/TRO.2022.3231360.
[30] M. T. Chikhaoui, B. Rosa, *Endorobotics*, Academic Press, Cambridge **2022**, pp. 187–213, https://doi.org/10.1016/B978-0-12-821750-4.00008-6.
[31] X. Wang, Y. Li, K. W. Kwok, *Front. Rob. AI* **2021**, *8*, 730330.
[32] C. Shi, X. Luo, P. Qi, T. Li, S. Song, Z. Najdovski, T. Fukuda, H. Ren, *IEEE Trans. Biomed. Eng.* **2017**, *64*, 1665.
[33] H. Wang, M. Totaro, L. Beccai, *Adv. Sci.* **2018**, *5*, 1800541.
[34] J. Burgner-Kahrs, D. C. Rucker, H. Choset, *IEEE Trans. Rob.* **2015**, *31*, 1261.
[35] P. Dupont, N. Simaan, H. Choset, C. Rucker, in *Proc. IEEE*, IEEE, Piscataway, NJ **2022**, https://doi.org/10.1109/JPROC.2022.3141338.
[36] T. da Veiga, J. H. Chandler, P. Lloyd, G. Pittiglio, N. J. Wilkinson, A. K. Hoshiar, R. A. Harris, P. Valdastri, *Prog. Biomed. Eng.* **2020**, *2*, 032003.
[37] K. Xu, J. Zhao, M. Fu, *IEEE/ASME Trans. Mechatron.* **2015**, *20*, 2133.
[38] C. B. Black, J. Till, D. C. Rucker, *IEEE Trans. Rob.* **2017**, *34*, 29.
[39] M. Dehghani, S. A. A. Moosavian, in *Proc. RSI/ISM Int. Conf. Robotics and Mechatronics*, Tehran, Iran **2013**, pp. 14–19.

[40] J. Starke, E. Amanov, M. T. Chikhaoui, J. Burgner-Kahrs, in *Proc. IEEE/RSJ Int. Conf. Intelligent Robots and Systems*, Vancouver, Canada **2017**, pp. 6470–6476.
[41] C. Li, C. D. Rahn, *ASME J. Mech. Des.* **2002**, *124*, 265.
[42] E. Amanov, T. D. Nguyen, J. Burgner-Kahrs, *Int. J. Rob. Res.* **2019**, *40*, 7.
[43] R. J. Murphy, M. D. Kutzer, S. M. Segreti, B. C. Lucas, M. Armand, *Robotica* **2014**, *32*, 835.
[44] T. Hassan, B. Mazzolai, C. Laschi, P. Dario, in *Proc. IEEE/RSJ Int. Conf. Intelligent Robots and Systems*, Vancouver, Canada **2017**.
[45] X. Dong, M. Raffles, S. Cobos-Guzman, D. Axinte, J. Kell, *J. Mech. Rob.* **2016**, *8*, 021010.
[46] M. Russo, L. Raimondi, X. Dong, D. Axinte, J. Kell, *Rob. Comput.-Integr. Manuf.* **2021**, *1*, 102096.
[47] P. Qi, C. Qiu, H. Liu, J. S. Dai, L. Seneviratne, K. Althoefer, *IEEE/ASME Trans. Mechatron.* **2016**, *21*, 1281.
[48] Y. Kim, S. S. Cheng, M. Diakite, R. P. Gullapalli, J. M. Simard, J. P. Desai, *IEEE Trans. Rob.* **2017**, *33*, 1386.
[49] M. Li, R. Kang, S. Geng, E. Guglielmino, *Trans. Inst. Meas.* **2018**, *40*, 3263.
[50] D. C. Rucker, B. A. Jones, R. J. Webster, in *Proc. IEEE Int. Conf. Robotics and Automation*, IEEE, Piscataway, NJ **2010**, pp. 1047–1052.
[51] Q. Peyron, K. Rabenorosoa, N. Andreff, P. Renaud, *Mech. Mach. Theory* **2019**, *132*, 176.
[52] C. Girerd, K. Rabenorosoa, P. Rougeot, P. Renaud, in *Proc. IEEE/RSJ Int. Conf. Intelligent Robots and Systems*, Vancouver, BC, Canada **2017**, pp. 5661–5887.
[53] C. Girerd, T. Schlinquer, N. Andreff, P. Renaud, K. Rabenorosoa, *J. Mech. Rob.* **2021**, *13*, 011006.
[54] K. Oliver-Butler, J. A. Childs, A. Daniel, D. C. Rucker, *IEEE Trans. Rob.* **2021**, *38*, 1186.
[55] Z. Mitros, S. M. H. Sadati, S. Nousias, L. Da Cruz, C. Bergeles, in *Proc. IEEE Int. Conf. Robotics and Automation*, Philadelphia **2022**.
[56] G. Del Giudice, L. Wang, J.-H. Shen, K. Joos, N. Simaan, in *Proc. IEEE/RSJ Int. Conf. Intelligent Robots and Systems*, Vancouver, BC, Canada **2017**, pp. 2537–2542.
[57] T. H. Fass, R. Cahill, M. Khan, G. Hao, P. Cantillon-Murphy, *Minimally Invasive Ther. Allied Technol.* **2022**, *31*, 1050.
[58] F. Leong, N. Garbin, C. Di Natali, A. Mohammadi, D. Thiruchelvam, D. Oetomo, P. Valdastri, *IEEE Rev. Biomed. Eng.* **2016**, *9*, 66.
[59] W. Felt, M. J. Telleria, T. F. Allen, G. Hein, J. B. Pompa, K. Albert, C. D. Remy, *Auton. Rob.* **2019**, *43*, 435.
[60] K. Althoefer, *Nat. Rev. Mater.* **2018**, *3*, 76.
[61] V. Falkenhahn, A. Hildebrandt, R. Neumann, O. Sawodny, *IEEE/ASME Trans. Mechatron.* **2017**, *22*, 6.
[62] L. H. Blumenschein, L. T. Gan, J. A. Fan, A. M. Okamura, E. W. Hawkes, *IEEE Rob. Autom. Lett.* **2018**, *3*, 94.
[63] P. Berthet-Rayne, S. H. Sadati, G. Petrou, N. Patel, S. Giannarou, D. R. Leff, C. Bergeles, *IEEE Rob. Autom. Lett.* **2021**, *6*, 5056.
[64] Z. Wu, M. D. I. Reyzabal, S. H. Sadati, H. Liu, S. Ourselin, D. Leff, R. K. Katzschmann, K. Rhode, C. Bergeles, *IEEE Rob. Autom. Lett.* **2023**, *8*, 1005.
[65] S. K. Talas, B. A. Baydere, T. Altinsoy, C. Tutcu, E. Samur., *Soft Rob.* **2020**, *7*, 521.
[66] C. Tutcu, B. A. Baydere, S. K. Talas, E. Samur, *Int. J. Rob. Res.* **2021**, *40*, 86.
[67] K. Oliver-Butler, J. Till, C. Rucker, *IEEE Trans. Rob.* **2019**, *35*, 403.
[68] D. Ji, T. H. Kang, S. Shim, J. Hong, *Int. J. Control Autom. Syst.* **2020**, *18*, 10.
[69] Y. Zhao, Y. Shan, J. Zhang, K. Guo, L. Qi, L. Han, H. Yu, *Bioinspiration Biomimetics* **2019**, *14*, 66007.
[70] M. Langer, E. Amanov, J. Burgner-Kahrs, *Soft Rob.* **2018**, *5*, 291.
[71] Y. Fang, C. Bishop, W. Ba, J. Barrientos Díez, A. Mohammad, X. Dong, in *Towards Autonomous and Robotic Systems, 21st Conf., TAROS 2020*, Springer, Nottingham, UK **2020**.
[72] F. Alambeigi, R. Seifabadi, M. Armand, in *Proc. IEEE Int. Conf. Robotics and Automation*, IEEE, Piscataway, NJ **2016**, pp. 758–764.
[73] A. Firouzeh, S. S. M. Salehian, A. Billard, J. Paik, in *Proc. IEEE Int. Conf. Robotics and Automation*, IEEE, Piscataway, NJ **2015**, pp. 2536–2543.
[74] C. Yang, S. Geng, I. Walker, D. T. Branson, J. Liu, J. S. Dai, R. Kang, *Int. J. Rob. Res.* **2020**, *39*, 1620.
[75] C. Abah, A. L. Orekhov, N. Simaan, in *Proc. IEEE Int. Conf. Robotics and Automation*, Brisbane, Australia **2018**, pp. 767–774.
[76] C. Bishop, M. Russo, X. Dong, D. Axinte, *IEEE/ASME Trans. Mechatron.* **2022**, *27*, 5339.
[77] B. Zhao, W. Zhang, Z. Zhang, X. Zhu, K. Xu, in *Proc. IEEE/RSJ Int. Conf. Intelligent Robots and Systems*, Madrid, Spain **2018**, pp. 7492–7499.
[78] B. Zhao, L. Zeng, B. Wu, K. Xu, in *Proc. IEEE Int. Conf. Robotics and Automation*, Paris, France **2020**, pp. 1847–1853.
[79] J. Kim, W.-Y. Choi, S. Kang, C. Kim, K.-J. Cho, *IEEE Trans. Rob.* **2019**, *35*, 1475.
[80] C. B. Black, D. C. Rucker, in *Proc. IEEE Int. Conf. Robotics and Automation*, IEEE, Piscataway, NJ **2014**, pp. 778–785.
[81] S. Lilge, K. Nülle, G. Böttcher, S. Spindeldreier, J. Burgner-Kahrs, *J. Mech. Rob.* **2020**, *13*, article no. 011025.
[82] M. Ghafoori, A. K. Khalaji, *Rob. Auton. Syst.* **2020**, *134*, 103650.
[83] B. Mauzé, R. Dahmouche, G. J. Laurent, A. N. André, P. Rougeot, P. Sandoz, C. Clévy, *IEEE Rob. Autom. Lett.* **2020**, *5*, 3806.
[84] P. H. Nguyen, C. Sparks, S. G. Nuthi, N. M. Vale, P. Polygerinos, *Soft Rob.* **2018**, *6*, 38.
[85] Z. Mitros, S. Sadati, C. Seneci, E. Bloch, K. Leibrandt, M. Khadem, L. Da Cruz, C. Bergeles, *IEEE Robot. Autom. Lett.* **2020**, *5*, 4874.
[86] M. Russo, N. Sriratanasak, W. Ba, X. Dong, A. Mohammad, D. Axinte, *IEEE Rob. Autom. Lett.* **2022**, *7*, 1558.
[87] P. Liljebäck, K. Y. Pettersen, Ø. Stavdahl, J. T. Gravdahl, *Rob. Auton. Syst.* **2012**, *1*, 29.
[88] P. R. Slawinski, A. Z. Taddese, K. B. Musto, S. Sarker, P. Valdastri, K. L. Obstein, *Gastroenterology* **2018**, *6*, 1577.
[89] G. Pittiglio, P. Lloyd, T. da Veiga, O. Onaizah, C. Pompili, J. H. Chandler, P. Valdastri, *Soft Rob.* **2022**, *9*, 1120.
[90] M. Russo, *Robotics* **2023**, *12*, 4.
[91] J. Barrientos-Diez, M. Russo, X. Dong, D. Axinte, J. Kell, *IEEE Rob. Autom. Lett.* **2023**, https://doi.org/10.1109/LRA.2023.3238890.
[92] L. Wu, R. Crawford, J. Roberts, *IEEE Rob. Autom. Lett.* **2016**, *2*, 514.
[93] J. Wang, H. Y. Lau, *J. Mech. Rob.* **2021**, *13*, 1.
[94] E. Gautreau, X. Bonnet, T. Fox, G. Fosseries, V. Valle, A. Herrel, M. A. Laribi, *J. Bionic Eng.* **2022**, article no. 061012.
[95] E. Gautreau, X. Bonnet, J. Sandoval, G. Fosseries, A. Herrel, M. Arsicault, S. Zeghloul, M. A. Laribi, *Biomimetics* **2022**, *7*, 223.
[96] X. Huang, J. Zou, G. Gu, *IEEE/ASME Trans. Mechatron.* **2021**, *26*, 3175.
[97] A. A. Shabana, A. E. Eldeeb, *Nonlinear Dyn.* **2021**, *104*, 165.
[98] S. M. H. Sadati, S. E. Naghibi, A. Shiva, B. Michael, L. Renson, M. Howard, C. D. Rucker, K. Althoefer, T. Nanayakkara, S. Zschaler, C. Bergeles, *Int. J. Rob. Res.* **2020**, *40*, 296.
[99] F. Boyer, V. Lebastard, F. Candelier, F. Renda, *IEEE Trans. Rob.* **2021**, *37*, 847.
[100] D. Trivedi, A. Lotfi, C. D. Rahn, *IEEE Trans. Rob.* **2008**, *24*, 773.
[101] D. C. Rucker, R. J. Webster III, *IEEE Trans. Rob.* **2011**, *27*, 1033.
[102] J. Till, V. Aloi, C. Rucker, *Int. J. Rob. Res.* **2019**, *38*, 723.
[103] M. Gazzola, L. H. Dudte, A. G. McCormick, L. Mahadevan, *R. Soc. Open Sci.* **2018**, *5*, 171628.

[104] S. M. Mustaza, Y. Elsayed, C. Lekakou, C. Saaj, J. Fras, *Soft Rob.* **2019**, *6*, 305.
[105] A. L. Orekhov, N. Simaan, in *Proc. IEEE/RSJ Int. Conf. Intelligent Robots and Systems*, IEEE, Piscataway, NJ **2020**, pp. 8653–8660.
[106] C. Della Santina, D. Rus, *IEEE Rob. Autom. Lett.* **2020**, *5*, 290.
[107] C. Della Santina, A. Bicchi, D. Rus, *IEEE Rob. Autom. Lett.* **2020**, *5*, 1001.
[108] G. S. Chirikjian, J. W. Burdick, *IEEE Trans. Rob. Autom.* **1994**, *10*, 343.
[109] G. S. Chirikjian, *J. Intell. Rob. Syst.* **1997**, *19*, 5.
[110] G. S. Chirikjian, J. W. Burdick, *IEEE Trans. Rob. Autom.* **1995**, *11*, 781.
[111] S. M. H. Sadati, S. E. Naghibi, I. D. Walker, K. Althoefer, T. Nanayakkara, *IEEE Rob. Autom. Lett.* **2018**, *3*, 328.
[112] S. M. H. Sadati, Z. Mitros, R. Henry, L. Zeng, L. Da Cruz, C. Bergeles, *IEEE Rob. Autom. Lett.* **2022**, *7*, 5671.
[113] I. Singh, Y. Amara, A. Melingui, P. Mani Pathak, R. Merzouki, *Soft Rob.* **2018**, *5*, 425.
[114] I. S. Godage, D. T. Branson, E. Guglielmino, G. A. Medrano-Cerda, D. G. Caldwell, in *Proc. IEEE Int. Conf. Robotics and Automation*, Shanghai, China **2011**, pp. 452–457.
[115] I. S. Godage, E. Guglielmino, D. T. Branson, G. A. Medrano-Cerda, D. G. Caldwell, in *Proc. IEEE/RSJ Int. Conf. Intelligent Robots and Systems*, San Francisco, CA **2011**, pp. 1093–1098.
[116] S. M. H. Sadati, S. E. Naghibi, A. Shiva, Y. Noh, A. Gupta, I. D. Walker, K. Althoefer, T. Nanayakkara, *Front. Rob. AI* **2017**, *4*, 22.
[117] S. M. H. Sadati, S. E. Naghibi, A. Shiva, I. D. Walker, K. Althoefer, T. Nanayakkara, *Towards Autonomous Robotic Systems*, Vol. *10454*, Springer, Surrey, UK **2017**, pp. 686–702.
[118] C. Della Santina, R. K. Katzschmann, A. Bicchi, D. Rus, *Int. J. Rob. Res.* **2020**, *39*, 490.
[119] A. Shiva, S. H. Sadati, Y. Noh, J. Fraś, A. Ataka, H. Würdemann, H. Hauser, I. D. Walker, T. Nanayakkara, K. Althoefer, *Soft Rob.* **2019**, *6*, 228.
[120] F. Renda, F. Boyer, J. Dias, L. Seneviratne, *IEEE Trans. Rob.* **2018**, *34*, 1518.
[121] E. Coevoet, T. Morales-Bieze, F. Largilliere, Z. Zhang, M. Thieffry, M. Sanz-Lopez, B. Carrez, D. Marchal, O. Goury, J. Dequidt, C. Duriez, *Adv. Rob.* **2017**, *31*, 1208.
[122] F. Renda, F. Giorgio-Serchi, F. Boyer, C. Laschi, J. Dias, L. Seneviratne, *Int. J. Rob. Res.* **2018**, *37*, 648.
[123] C. Rucker, *IEEE Rob. Autom. Lett.* **2018**, *3*, 2979.
[124] S. Grazioso, G. Di Gironimo, B. Siciliano, *Soft Rob.* **2019**, *6*, 790.
[125] I. Singh, *Curve Based Approach for Shape Reconstruction of Continuum Manipulators*, Universite de Lille, Lille, France **2018**.
[126] G. S. Chirikjian, in *Proc. IEEE/RSJ Int. Conf. Intelligent Robots and Systems*, Vol. *2*, IEEE, Piscataway, NJ **1993**, pp. 1059–1066.
[127] M. Thieffry, A. Kruszewski, T.-M. Guerra, C. Duriez, in *2018 European Control Conf. (ECC)*, Limassol **2018**, pp. 635–640.
[128] M. Thieffry, A. Kruszewski, T.-M. Guerra, C. Duriez, *IEEE Trans. Control Syst. Technol.* **2019**, *29*, 556.
[129] M. Thieffry, A. Kruszewski, C. Duriez, T. Guerra, *IEEE Rob. Autom. Lett.* **2018**, *4*, 25.
[130] J. Chenevier, D. González, J. V. Aguado, F. Chinesta, E. Cueto, *Plos One* **2018**, *13*, e0192052.
[131] H. Wegiriya, N. Herzig, S.-A. Abad, S. M. H. Sadati, T. Nanayakkara, *IEEE Sens. J.* **2019**, 10.
[132] Y. Shapiro, A. Wolf, K. Gabor, *Sens. Actuators, A* **2011**, *167*, 484.
[133] I. S. Godage, G. A. Medrano-Cerda, D. T. Branson, E. Guglielmino, D. G. Caldwell, *Int. J. Rob. Res.* **2016**, *35*, 695.
[134] H. Habibi, C. Yang, I. S. Godage, R. Kang, I. D. Walker, D. T. Branson, *J. Mech. Rob.* **2020**, *12*, 011014.
[135] I. S. Godage, R. Wirz, I. D. Walker, R. J. Webster, *Soft Rob.* **2015**, *2*, 96.
[136] T. Gopesh, J. Friend, *Soft Rob.* **2020**, *8*, 365.
[137] J. Till, V. Aloi, K. E. Riojas, P. L. Anderson, R. J. Webster III, C. Rucker, *IEEE Trans. Rob.* **2020**, *36*, 1704.
[138] B. Caasenbrood, A. Pogromsky, H. Nijmeijer, *Soft Rob.* **2022**, https://doi.org/10.1089/soro.2021.0035.
[139] Y. Liu, F. Alambeigi, *IEEE Rob. Autom. Lett.* **2021**, *6*, 1606.
[140] H. Yuan, L. Zhou, W. Xu, *Mech. Mach. Theory* **2019**, *135*, 130.
[141] J. Ha, F. C. Park, P. E. Dupont, in *Proc. IEEE/RSJ Int. Conf. Intelligent Robots and Systems*, IEEE, Piscataway, NJ **2014**, pp. 864–870.
[142] J. Till, D. C. Rucker, *IEEE Trans. Rob.* **2017**, *33*, 718.
[143] S. M. H. Sadati, A. Shiva, N. Herzig, C. D. Rucker, H. Hauser, I. D. Walker, C. Bergeles, K. Althoefer, T. Nanayakkara, *IEEE Rob. Autom. Lett.* **2020**, *5*, 2824.
[144] R. Xu, A. Asadian, A. S. Naidu, R. V. Patel, in *Proc. IEEE Int. Conf. Robotics and Automation*, IEEE, Piscataway, NJ **2013**, pp. 5813–5818.
[145] A. Munawar, N. Srishankar, G. S. Fischer, in *Proc. IEEE Int. Conf. Robotics and Automation*, Paris, France **2020**, p. 7.
[146] T. M. Bieze, F. Largilliere, A. Kruszewski, Z. Zhang, R. Merzouki, C. Duriez, *Soft Rob.* **2018**, *5*, 348.
[147] C. Duriez, T. Bieze, *Soft Robotics: Trends, Applications and Challenges*, Vol. *17*, Springer International Publishing, Cham **2017**, pp. 103–109.
[148] W. Huang, X. Huang, C. Majidi, M. K. Jawed, *Nat. Commun.* **2020**, *11*, 2233.
[149] G. S. Chirikjian, *J. Mech. Des.* **1995**, *117*, 347.
[150] I. Tunay, *IEEE Trans. Rob.* **2013**, *29*, 297.
[151] O. Goury, C. Duriez, *IEEE Trans. Rob.* **2018**, *34*, 1565.
[152] J. Collins, S. Chand, A. Vanderkop, D. Howard, *IEEE Access* **2021**, *9*, 16.
[153] N. Naughton, J. Sun, A. Tekinalp, G. Chowdhary, M. Gazzola, *IEEE Rob. Autom. Lett.* **2021**, *6*, 3389.
[154] Y. Hu, J. Liu, A. Spielberg, J. B. Tenenbaum, W. T. Freeman, J. Wu, D. Rus, W. Matusik, in *Proc. IEEE Int. Conf. Robotics and Automation*, IEEE, Piscataway, NJ, May 2019, pp. 6265–6271.
[155] M. Li, Z. Ferguson, T. Schneider, T. R. Langlois, D. Zorin, D. Panozzo, C. Jiang, D. M. Kaufman, *ACM Trans. Graphics* **2020**, *39*, 49.
[156] M. A. Graule, C. B. Teeple, T. P. McCarthy, G. R. Kim, R. C. St. Louis, R. J. Wood, in *Proc. IEEE/RSJ Int. Conf. Intelligent Robots and Systems*, IEEE, Piscataway, NJ, September 2021, pp. 3934–3941.
[157] A. Munawar, Y. Wang, R. Gondokaryono, G. S. Fischer, in *Proc. IEEE/RSJ Int. Conf. Intelligent Robots and Systems*, IEEE, Piscataway, NJ **2019**, pp. 1875–1882.
[158] J. M. Bern, D. Rus, in *2021 IEEE 4th Int. Conf. Soft Robotics (RoboSoft)*, IEEE, Piscataway, NJ, April 2021, pp. 465–471, https://doi.org/10.1109/robosoft51838.2021.9479195.
[159] A. T. Mathew, I. B. Hmida, F. Renda, arXiv preprint arXiv:2107.05494, **2021**.
[160] K. P. Ashwin, A. Ghosal, *Mechanism and Machine Science*, Springer, Singapore **2018**, pp. 391–403.
[161] L. Wang, N. Simaan, *IEEE Trans. Rob.* **2019**, *35*, 387.
[162] M. Giorelli, F. Renda, M. Calisti, A. Arienti, G. Ferri, C. Laschi, *IEEE Trans. Rob.* **2015**, *31*, 823.
[163] K. H. Lee, D. K. Fu, M. C. Leong, M. Chow, H. C. Fu, K. Althoefer, K. Y. Sze, C. K. Yeung, K. W. Kwok, *Soft Rob.* **2017**, *4*, 324.
[164] A. Kuntz, A. Sethi, R. J. Webster, R. Alterovitz, *IEEE Trans. Med. Rob. Bionics* **2020**, *2*, 140.
[165] D. Bruder, X. Fu, R. B. Gillespie, C. D. Remy, R. Vasudevan, *IEEE Trans. Rob.* **2021**, *37*, 948.
[166] A. W. Mahoney, T. L. Bruns, P. J. Swaney, R. J. Webster, III, in *Proc. IEEE Int. Conf. Robotics and Automation*, Stockholm, Sweden, May 2016, pp. 4472–4478.
[167] M. M. Dalvand, S. Nahavandi, R. D. Howe, *Phys. Med. Biol.* **2016**, *61*, 5128.
[168] T. Mahl, A. Hildebrandt, O. Sawodny, *IEEE Trans. Rob.* **2014**, *30*, 935.

[169] T. Poignonec, P. Zanne, B. Rosa, F. Nageotte, *IEEE Rob. Autom. Lett.* **2020**, *5*, 4788.
[170] M. Hofer, C. Sferrazza, R. D'Andrea, *Front. Rob. AI* **2021**, *8*, 8.
[171] M. Ho, Y. Kim, S. S. Cheng, R. Gullapalli, J. P. Desai, *Int. J. Rob. Res.* **2015**, *34*, 1147.
[172] H. Guo, F. Ju, Y. Cao, F. Qi, D. Bai, Y. Wang, B. Chen, *Sens. Actuators, A* **2019**, *285*, 519.
[173] N. Rahman, N. J. Deaton, J. Sheng, S. S. Cheng, J. P. Desai, *IEEE Rob. Autom. Lett.* **2019**, *4*, 1424.
[174] R. J. Roesthuis, S. Misra, *IEEE Trans. Rob.* **2016**, *32*, 372.
[175] F. Alambeigi, S. A. Pedram, J. L. Speyer, J. Rosen, I. Iordachita, R. H. Taylor, M. Armand, *IEEE Trans. Rob.* **2019**, *36*, 222.
[176] F. Khan, A. Denasi, D. Barrera, J. Madrigal, S. Sales, S. Misra, *IEEE Sens. J.* **2019**, *19*, 5878.
[177] H. Bai, S. Li, J. Barreiros, Y. Tu, C. R. Pollock, R. F. Shepherd, *Science* **2020**, *370*, 848.
[178] M. Luo, Y. Pan, E. H. Skorina, W. Tao, F. Chen, S. Ozel, C. D. Onal, *Bioinspiration Biomimetics* **2015**, *10*, 055001.
[179] H. Zhao, K. O'Brien, S. Li, R. F. Shepherd, *Sci. Rob.* **2016**, *1*, eaai7529.
[180] S. Hamill, J. Whitehead, P. Ferenz, R. F. Shepherd, H. Kress-Gazit, in *Proc. IEEE Int. Conf. Robotics and Automation*, IEEE, Piscataway, NJ **2019**, pp. 5148–5154.
[181] Y. Shapiro, G. Kósa, A. Wolf, *IEEE/ASME Trans. Mechatron.* **2013**, *19*, 1260.
[182] D. Alatorre, D. Axinte, A. Rabani, *IEEE Trans. Rob.* **2022**, *38*, 526.
[183] S. Yao, Y. Zhu, *Nanoscale* **2014**, *6*, 2345.
[184] J. Shintake, Y. Piskarev, S. H. Jeong, D. Floreano, *Adv. Mater. Technol.* **2018**, *3*, 1700284.
[185] S. Cheng, Y. S. Narang, *Adv. Mater. Interfaces* **2019**, *6*, 1900985.
[186] R. L. Truby, C. D. Santina, D. Rus, *IEEE Rob. Autom. Lett.* **2020**, *5*, 3299.
[187] D. C. Rucker, R. J. Webster III, in *Proc. IEEE/RSJ Int. Conf. Intelligent Robots and Systems*, San Francisco, CA **2011**, pp. 3764–3769.
[188] H. Yuan, P. W. Y. Chiu, Z. Li, *IEEE Rob. Autom. Lett.* **2017**, *2*, 1972.
[189] M. Khoshnam, A. C. Skanes, R. V. Patel, *IEEE Trans. Biomed. Eng.* **2015**, *62*, 1404.
[190] J. Back, L. Lindenroth, R. Karim, K. Althoefer, K. Rhode, H. Liu, in *Proc. IEEE/RSJ Int. Conf. Intelligent Robots and Systems*, Daejeon, Korea **2016**, pp. 2122–2127.
[191] S. Hasanzadeh, F. Janabi-Sharifi, *IEEE/ASME Trans. Mechatron.* **2016**, *21*, 154.
[192] K. Xu, N. Simaan, *IEEE Trans. Robot.* **2008**, *24*, 576.
[193] K. Xu, N. Simaan, *IEEE Trans. Robot.* **2010**, *26*, 555.
[194] R. E. Goldman, A. Bajo, N. Simaan, *IEEE Trans. Rob.* **2014**, *30*, 890.
[195] A. Bajo, N. Simaan, *Int. J. Rob. Res.* **2015**, *35*, 422.
[196] R. Yasin, N. Simaan, *Int. J. Rob. Res.* **2020**, *40*, 764.
[197] D. Haraguchi, T. Kanno, K. Tadano, K. Kawashima, *IEEE/ASME Trans. Mechatron.* **2015**, *20*, 2950.
[198] R. Xu, A. Yurkewich, R. V. Patel, *IEEE Rob. Autom. Lett.* **2016**, *1*, 1052.
[199] F. Khan, R. J. Roesthuis, S. Misra, in *Proc. IEEE/RSJ Int. Conf. Intelligent Robots and Systems*, Vancouver, BC, Canada **2017**, pp. 2531–2536.
[200] W. Lai, L. Cao, R. X. Tan, P. T. Phan, J. Hao, S. C. Tjin, S. J. Phee, *IEEE/ASME Trans. Mechatron.* **2020**, *25*, 371.
[201] L. Scimeca, J. Hughes, P. Maiolino, F. Iida, *IEEE Rob. Autom. Lett.* **2019**, *4*, 2479.
[202] J. Ha, P. E. Dupont, *IEEE Rob. Autom. Lett.* **2017**, *2*, 298.
[203] K. E. Riojas, R. J. Hendrick, R. J. Webster, *IEEE Rob. Autom. Lett.* **2018**, *3*, 1624.
[204] A. M. Okamura, *Ind. Robot* **2004**, *31*, 499.
[205] M. Csencsits, B. A. Jones, W. McMahan, V. Iyengar, I. D. Walker, in *Proc. IEEE/RSJ Int. Conf. Intelligent Robots and Systems*, Edmonton, AB, Canada **2005**, pp. 3123–3130.
[206] A. D. Kapadia, I. D. Walker, E. Tatlicioglu, in *Proc. IEEE/RSJ Int. Conf. Intelligent Robots and Systems*, Vilamoura, Algarve, Portugal **2012**, pp. 3105–3110.
[207] C. G. Frazelle, A. D. Kapadia, K. E. Fry, I. D. Walker, in *Proc. IEEE Int. Conf. Robotics and Automation*, Stockholm, Sweden **2016**, pp. 4093–4100.
[208] B. Zhao, S. A. Zhang, Z. Wu, B. Yang, K. Xu, *Int. J. Med. Rob.* **2020**, *16*, e2042.
[209] H.-S. Yoon, B.-J. Yi, *Proc. Inst. Mech. Eng., Part C: J. Mech. Eng. Sci.* **2017**, *231*, 1921.
[210] C. G. Frazelle, A. Kapadia, I. Walker, *J. Mech. Rob.* **2018**, *10*, 025005.
[211] C. G. Frazelle, A. D. Kapadia, I. D. Walker, *IEEE Rob. Autom. Lett.* **2020**, *5*, 1875.
[212] J. S. Mehling, M. A. Diftler, M. Chu, M. Valvo, in *Proc. IEEE RAS EMBS Int. Conf. Biomedical Robotics and Biomechatronics*, IEEE, Piscataway, NJ **2006**, pp. 690–695.
[213] S. Liu, Z. Yang, Z. Zhu, L. Han, X. Zhu, K. Xu, *Ind. Robot* **2016**, *43*, 284.
[214] A. Ataka, A. Shiva, H. K. Lam, K. Althoefer, in *Proc. IEEE/RSJ Int. Conf. Intelligent Robots and Systems*, Madrid, Spain **2018**, pp. 168–173.
[215] H. Choset, W. Henning, *Int. J. Aerosp. Eng.* **1999**, *12*, 65.
[216] H. B. Gilbert, J. Neimat, *IEEE Trans. Rob.* **2015**, *31*, 246.
[217] Y. Gao, K. Takagi, T. Kato, N. Shono, N. Hata, *IEEE Trans. Biomed. Eng.* **2020**, *67*, 379.
[218] L. Dupourqué, F. Masaki, Y. L. Colson, T. Kato, N. Hata, *Int. J. Comput. Assisted Radiol. Surg.* **2019**, *14*, 2021.
[219] M. Wang, X. Dong, W. Ba, A. Mohammad, D. Axinte, A. Norton, *Rob. Comput. Integr. Manuf.* **2020**, *67*, 102054.
[220] B. Kang, R. Kojcev, E. Sinibaldi, *PloS One* **2016**, *11*, e0150278.
[221] M. Neumann, J. Burgner-Kahrs, in *Proc. IEEE Int. Conf. Robotics and Automation*, Stockholm, Sweden **2016**, pp. 917–923.
[222] P. W. J. Henselmans, C. Culmone, D. J. Jager, R. I. B. van Starkenburg, P. Breedveld, *Med. Eng. Phys.* **2020**, *86*, 86.
[223] C. Bergeles, A. H. Gosline, N. V. Vasilyev, P. J. Codd, J. Pedro, P. E. Dupont, *IEEE Trans. Rob.* **2015**, *31*, 67.
[224] A. Garriga-Casanovas, F. Rodriguez y Baena, *Int. J. Rob. Res.* **2018**, *37*, 197.
[225] C. Girerd, A. V. Kudryavtsev, P. Rougeot, P. Renaud, K. Rabenorosoa, B. Tamadazte, *IEEE Rob. Autom. Lett.* **2020**, *5*, 548.
[226] S. Isnard, W. K. Silk, *Am. J. Bot.* **2009**, *96*, 1205.
[227] E. D. Dottore, A. Mondini, A. Sadeghi, V. Mattoli, B. Mazzolai, in *Proc. IEEE Int. Conf. Robotics and Automation*, Stockholm, Sweden **2016**, pp. 4722–4728.
[228] M. B. Wooten, I. D. Walker, *Robotics* **2018**, *7*, 58.
[229] M. Wooten, C. Frazelle, I. D. Walker, A. Kapadia, J. H. Lee, in *Proc. IEEE Int. Conf. Robotics and Automation*, Brisbane, QLD, Australia **2018**, pp. 5526–5533.
[230] A. Sadeghi, A. Mondini, E. Del Dottore, V. Mattoli, L. Beccai, S. Taccola, C. Lucarotti, M. Totaro, B. Mazzolai, *Bioinspiration Biomimetics* **2016**, *12*, 015001.
[231] E. Del Dottore, A. Sadeghi, A. Mondini, B. Mazzolai, in *Proc. IEEE Int. Conf. Robotics and Automation*, Brisbane, Australia **2018**, pp. 3454–3460.
[232] B. Mazzolai, F. Tramacere, I. Fiorello, L. Margheri, *Front. Rob. AI* **2020**, *7*, 130.
[233] M. Selvaggio, L. A. Ramirez, N. D. Naclerio, B. Siciliano, E. W. Hawkes, in *Proc. IEEE Int. Conf. Robotics and Automation*, Paris, France **2020**, pp. 3227–3233.
[234] J. D. Greer, L. H. Blumenschein, A. M. Okamura, E. W. Hawkes, in *Proc. IEEE Int. Conf. Robotics and Automation*, Brisbane, Australia **2018**, pp. 4165–4172.
[235] I. Fiorello, E. Del Dottore, F. Tramacere, B. Mazzolai, *Bioinspiration Biomimetics* **2020**, *15*, 031001.

[236] J. Gallentine, M. B. Wooten, M. Thielen, I. D. Walker, T. Speck, K. Niklas, *Front. Rob. AI* **2020**, *7*, 1.
[237] W. McMahan, V. Chitrakaran, M. Csencsits, D. Dawson, I. D. Walker, B. A. Jones, M. Pritts, D. Dienno, M. Grissom, C. D. Rahn, in *IEEE Int. Conf. Advanced Robotics*, Orlando, FL **2006**, pp. 2336–2341.
[238] H. El-Hussieny, U. Mehmood, Z. Mehdi, S. G. Jeong, M. Usman, E. W. Hawkes, A. M. Okarnura, J. H. Ryu, in *Proc. IEEE/RSJ Int. Conf. Intelligent Robots and System*, Madrid, Spain **2018**, pp. 4995–5002.
[239] R. Vidoni, T. Mimmo, C. Pandolfi, *J. Bionic Eng.* **2015**, *12*, 250.
[240] A. Mohammad, M. Russo, Y. Fang, X. Dong, D. Axinte, J. Kell, *IEEE Robot. Autom. Lett.* **2021**, *6*, 7493.
[241] D. Palmer, D. Axinte, *Rob. Comput. Integr. Manuf.* **2019**, *56*, 107.
[242] H. Shi, M. Russo, J. de la Torre, X. Dong, A. Mohammad, D. Axinte, *IEEE Rob. Autom. Mag.* **2022**, 2, https://doi.org/10.1109/MRA.2022.3225718.
[243] X. Dong, M. Wang, A. Mohammad, M. Russo, W. Ba, A. Norton, J. Kell, D. Axinte, *IEEE/ASME Trans. Mechatron.* **2022**, *27*, 4217.
[244] D. Alatorre, J. A. Robles-Linares, M. Russo, M. A. Elbanna, S. Wild, X. Dong, A. Mohammad, J. Kell, A. D. Norton, D. Axinte, *IEEE Rob. Autom. Mag.* **2022**, 2, https://doi.org/10.1109/MRA.2022.3223220.
[245] H. Tsukagoshi, A. Kitagawa, M. Segawa, in *Proc. IEEE Int. Conf. Robotics and Automation*, Seoul, Korea **2001**, pp. 2454–2459.
[246] G. P. Scott, C. G. Henshaw, I. D. Walker, B. Willimon, in *Proc. IEEE/RSJ Int. Conf. Intelligent Robots and Systems*, Hamburg, Germany, October 2015, pp. 1664–1671.
[247] M. Srivastava, J. Ammons, A. B. Peerzada, V. N. Krovi, P. Rangaraju, I. D. Walker, in *Proc. IEEE Int. Conf. Robotics and Automation*, Philadelphia, PA, May 2022, pp. 3216–3222.
[248] R. E. Graham, R. E. Bostelman, in *ANS 7th Topical Meeting on Robotics and Remote Systems*, Augusta, GA **1997**, pp. 656–650.
[249] M. M. Coad, L. H. Blumenschein, S. Cutler, J. A. R. Zepeda, N. D. Naclerio, H. El-Hussieny, U. Mehmood, J. H. Ryu, E. W. Hawkes, A. M. Okamura, *IEEE Rob. Autom. Mag.* **2019**, *27*, 120.
[250] M. C. Lastinger, A. Rice, A. Kapadia, I. D. Walker, in *Proc. IEEE Aerospace Conf.*, Big Sky, MT **2020**, pp. 1–10.
[251] M. C. Lastinger, S. Verma, A. D. Kapadia, I. D. Walker, in *Proc. IEEE Int. Conf. Robotics and Automation*, Montreal, Canada, May 2019, pp. 5365–5371.
[252] P. A. der Maur, B. Djambazi, Y. Haberthür, P. Hörmann, A. Kübler, M. Lustenberger, S. Sigrist, O. Vigen, J. Förster, F. Achermann, E. Hampp, in *IEEE Int. Conf. Soft Robot (RoboSoft)*, IEEE, Piscataway, NJ **2021**, pp. 15–20.
[253] S. Kolachalama, S. Lakshmanan, *J. Rob.* **2020**, *2020*, 4187048.
[254] L. Chin, J. Lipton, M. C. Yuen, R. Kramer-Bottiglio, D. Rus, in *IEEE Int. Conf. Soft Robot (RoboSoft)*, IEEE, Piscataway, NJ **2019**, pp. 102–107.
[255] L. Chin, J. Lipton, R. MacCurdy, J. Romanishin, C. Sharma, D. Rus, in *IEEE Int. Conf. Soft Robot (RoboSoft)*, IEEE, Piscataway, NJ **2018**, pp. 100–107.
[256] A. Mehrkish, F. Janabi-Sharifi, *Mech. Mach. Theory* **2022**, *168*, 104575.
[257] A. Mehrkish, F. Janabi-Sharifi, *Rob. Auton. Syst.* **2021**, *145*, 103860.

Matteo Russo received the B.Sc., M.Sc., and Ph.D. degrees in mechanical engineering from the University of Cassino, Italy, in 2013, 2015, and 2019. He was a visiting researcher at RWTH Aachen University, Germany, University of the Basque Country, Spain, and Tokyo Institute of Technology, Japan. From 2019 to 2022, he was a research fellow at the University of Nottingham, UK, designing continuum robots for aerospace and nuclear. Currently, he is assistant professor at the University of Rome Tor Vergata, Italy. His research interests include continuum robots, mechanism design, robot kinematics, and parallel manipulators.

S. M. Hadi Sadati is a CME research fellow at the School of Biomedical Engineering & Imaging Sciences, King's College London, UK. He has a Ph.D. (2018) in robotics from King's College London, London, and has been a postdoc in robotics at King's College London, London (2019–2021), and in morphological computation at the University of Bristol (2017–2019). He was also a visiting researcher at LASA, EPFL (2019 and 2021), as well as the Prof. Walker's lab, Clemson University (2017), and Dyson School, Imperial College London (2016–2017). His research interests are soft medical robotics, morphological contribution, and system dynamics.

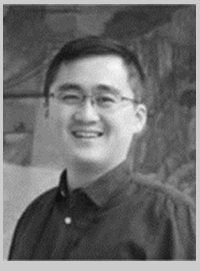

Xin Dong received his B.Eng. degree in mechanical engineering from Dalian University of Technology, Dalian, China, in 2008, the M.Eng. and Ph.D. degrees in mechatronics, robotics and automation engineering from Beihang University, Beijing, China, in 2011 and from University of Nottingham, Nottingham, UK, in 2015. He is currently an associate professor working at the University of Nottingham. His research interests are extra slender continuum robot and reconfigurable hexapod robots with novel actuation solutions for the application in aerospace, nuclear, oil and gas, and marine and rescue.

Abdelkhalick Mohammad received his B.Sc. degree in mechatronics engineering from Assiut University, Assiut, Egypt, in 2006, and the M.Eng. and Ph.D. degrees in robotics and mechatronics from Toyohashi University of Technology, Toyohashi, Japan, in 2010 and 2013, respectively. He is currently an assistant professor in mechatronics at the Department of Mechanical, Materials and Manufacturing Engineering, University of Nottingham, UK. His research interests include mechatronics system design, robotics, machine tool control, and control theory.

Ian D. Walker received the B.Sc. degree in mathematics from the University of Hull, UK, in 1983, and the M.S. and Ph.D. degrees, both in electrical engineering, in 1985 and 1989, respectively, from the University of Texas at Austin. He has served as Vice President for financial activities for the IEEE Robotics and Automation Society, and as Chair of the AIAA Technical Committee on Space Automation and Robotics. He has also served on the Editorial Boards of the IEEE Transactions on Robotics, the IEEE Transactions on Robotics and Automation, the International Journal of Robotics and Automation, the IEEE Robotics and Automation Magazine, and the International Journal of Environmentally Conscious Design and Manufacturing. He currently serves on the Editorial Board of Soft Robotics. Walker's research interests include biologically inspired and continuum robotics, as well as architectural robotics.

Christos Bergeles received the M.Sc. degree in electrical and computer engineering from the National Technical University of Athens, Athens, Greece, in 2006, and the Ph.D. degree in robotics from ETH Zurich, Zurich, Switzerland, in 2011. He is currently an associate professor (Reader) with King's College London, London, UK, where he directs the Robotics and Vision in Medicine Lab. Bergeles is the recipient of an ERC Starting Grant. He was an associate editor for the IEEE Transactions on Robotics and is associate editor for IEEE Robotics and Automation Letters. His research interests relate to image-guided robotic microsurgery and clinical translation.

Kai Xu received a B.E. and an M.S. from the Department of Precision Instruments and Mechanology, Tsinghua University, Beijing, China, in 2001 and 2004, respectively, and a Ph.D. (with distinction) from the Department of Mechanical Engineering, Columbia University, New York, NY, in 2009. He is now a professor with the School of Mechanical Engineering, Shanghai Jiao Tong University, Shanghai, China, and the director of the Robotics Innovation and Intervention Laboratory. His research interests include surgical robots, prosthetic hands, flexible manipulators, special industrial robots, and continuum mechanisms.

Dragos Axinte received the M.Eng. degree in manufacturing engineering in 1988, and the Ph.D. degree in manufacturing engineering in 1996. After graduating, he worked in R&D in industry for 10 years and then moved to academia to lead research in the field of machining, process monitoring and design of innovative tooling/robotics for in situ repair especially related to on-wing repair of aeroengines. Currently, he is professor of manufacturing engineering at University of Nottingham and Director of Rolls-Royce University Technology Centre (UTC) in Manufacturing and On-Wing Technology.